

1 **Modeling of the anthropogenic heat flux and its effect on**
2 **regional meteorology and air quality over the Yangtze River**
3 **Delta region, China**

4 Min Xie^{1*}, Jingbiao Liao¹, Tijian Wang^{1,2*}, Kuanguang Zhu¹, Bingliang Zhuang¹, Yong Han¹,
5 Mengmeng Li¹, Shu Li¹

6 ¹School of Atmospheric Sciences, Nanjing University, Nanjing, China;

7 ²CMA-NJU Joint Laboratory for Climate Prediction Studies, Institute for Climate and Global
8 Change Research, School of Atmospheric Sciences, Nanjing University, Nanjing, China

9

10 **Abstract:**

11 Anthropogenic heat (AH) emissions from human activities caused by urbanization can affect
12 the city environment. Based on the energy consumption and the gridded demographic data, the
13 spatial distribution of AH emission over the Yangtze River Delta (YRD) region is estimated.
14 Meanwhile, a new method for the AH parameterization is developed in the WRF/Chem model,
15 which incorporates the gridded AH emission data with the seasonal and the diurnal variations into
16 the simulations. By running this upgraded WRF/Chem for two typical months in 2010, the impacts
17 of AH on the meteorology and air quality over the YRD region are studied. The results show that
18 the AH fluxes over YRD have been growing in recent decades. In 2010, the annual mean values of
19 AH over Shanghai, Jiangsu and Zhejiang are 14.46, 2.61 and 1.63 W/m² respectively, with the
20 high values of 113.5 W/m² occurring in the urban areas of Shanghai. These AH emissions can
21 significantly change the urban heat island and urban-breeze circulations in the cities of the YRD
22 region. In Shanghai, 2-m air temperature increases by 1.6 °C in January and 1.4 °C in July, the
23 planetary boundary layer height rises up by 140m in January and 160m in July, and 10-m wind
24 speed is enhanced by 0.7 m/s in January and 0.5 m/s in July, with higher increment at night. The
25 enhanced vertical movement can transport more moisture to higher levels, which causes the
26 decrease of water vapor at the ground level and the increase in the upper PBL, and thereby induces
27 the accumulative precipitation to increase by 15-30% over the megacities in July. The adding AH
28 can impact the spatial and vertical distributions of the simulated pollutants as well. The
29 concentrations of primary air pollutants decrease near surface and increase at the upper levels, due

30 mainly to the increases of PBLH, surface wind speed and upward air vertical movement. But
31 surface O₃ concentrations increase in the urban areas, with maximum changes of 2.5ppb in
32 January and 4 ppb in July. Chemical direct (the rising up of air temperature directly accelerate
33 surface O₃ formation) and indirect (the decrease in NO_x at the ground results in the increase of
34 surface O₃) effects can play a significant role in O₃ changes over this region. The meteorology and
35 air pollution predictions in and around large urban areas are highly sensitive to the anthropogenic
36 heat inputs, suggesting that AH should be considered in the climate and air quality assessments.

37 **Key words:** Anthropogenic heat; WRF/Chem; Urban canopy model; Ozone; PM₁₀

38

39 -----

40 *Corresponding author, +86-25-89685302

41 E-mail address: minxie@nju.edu.cn, tjwang@nju.edu.cn

42

43 Nearly all energy used for human purposes can eventually turn into anthropogenic heat (AH)
44 within Earth's land-atmosphere system (Flanner, 2009; Chen et al., 2012). According to the
45 distinctive human activities all over the world, this heat flux might vary spatially and temporally.
46 On the global scale, the averaged value of AH flux has been estimated to be only 0.028 W/m². But
47 it can reach to 0.39, 0.68 and 0.22 W/m² respectively over the continental United States, Western
48 Europe and China (Flanner, 2009). In the densely populated and economically vibrant urban areas,
49 the AH fluxes have been reported to typically range from 20 to 70 W/m² (Crutzen, 2004; Sailor
50 and Lu, 2004; Fan and Sailor, 2005; Pigeon et al., 2007; Lee et al., 2009), whereas the fluxes
51 might occasionally exceed the value of 100 W/m² as well (Quah and Roth, 2012; Xie et al., 2015).
52 Under some extreme conditions, the magnitude of AH fluxes in cities can be a substantial heat
53 source equivalent to the daily mean solar forcing (Ichinose et al., 1999; Hamilton et al. 2009;
54 Iamarino et al. 2012), with a high value of 1590 W/m² reported in the densest part of Tokyo at the
55 peak of air-conditioning demand (Ichinose et al., 1999). Consequently, accurate prediction of AH
56 emissions is always a key issue that can improve our understanding of human impacts on urban
57 climate and environment.

58 Anthropogenic heat can increase turbulent fluxes in sensible and latent heat, which might
59 result in the atmosphere reserving more energy (Oke, 1988). Thus, the abovementioned heat

60 fluxes exhausted from human activities in cities can exert a significant influence on the dynamics
61 and thermodynamics of urban boundary layer (Ichinose et al., 1999; Block et al., 2004; Fan and
62 Sailor, 2005; Chen et al., 2009; Chen et al., 2012; Bohnenstengel et al., 2014), and thereby change
63 the surface meteorological conditions (Khan and Simpson, 2001; Block et al., 2004; Fan and
64 Sailor, 2005; Ferguson and Woodbury, 2007; Chen et al., 2009; Zhu et al., 2010; Menberg et al.,
65 2013; Wu and Yang, 2013; Feng et al., 2014; Bohnenstengel et al., 2014). Most previous studies of
66 AH have focused on these effects. For instance, some researchers have found that AH strengthens
67 the vertical movement of urban surface air flow, change the urban heat island circulation, and
68 make the urban boundary layer more turbulent and unstable (Ichinose et al., 1999; Block et al.,
69 2004; Fan and Sailor, 2005; Chen et al., 2009; Bohnenstengel et al., 2014). Others showed that AH
70 in cities can result in significant and extensive warming, and tend to cause urban air temperatures
71 to increase by several degrees (Fan and Sailor, 2005; Ferguson and Woodbury, 2007; Chen et al.,
72 2009; Zhu et al., 2010; Menberg et al., 2013; Wu and Yang, 2013; Feng et al., 2014;
73 Bohnenstengel et al., 2014). Moreover, Feng et al. (2014) reported that AH enhances the
74 convergence of water vapor and rainfall amounts over urbanized areas, and changes the regional
75 precipitation patterns to some extent. Urban air quality and local meteorological condition are
76 inextricably linked. Therefore, all the findings above are likely to have important implications for
77 air quality in urban areas as well. However, in the past, few researchers paid attention to this issue,
78 and only a couple of studies have estimated the effects of AH on air pollutants (Ryu et al., 2013;
79 Yu et al., 2014; Yang et al., 2014).

80 Over the past decades, along with the accelerated urbanization process and rapid economic
81 development, many cities in China have been suffering the successive deterioration of air quality
82 (Xie et al., 2014). Located in the coastal region in East China, the Yangtze River Delta (YRD)
83 region also experienced a rapid urban expansion with the urbanization rate as high as 70% and
84 suffered from air pollutions (Liao et al., 2015). Consequently, several previous studies have tried
85 to figure out the effects of urbanization on the severe atmospheric environmental problems in this
86 region. For example, by using WRF/Chem model, Wang et al. (2009) quantified that the urban
87 sprawl in YRD region has caused surface O₃ to increase by 2.9-4.2% during the daytime and
88 4.7-8.5% at night. **Employing** the WRF/CMAQ model, Li et al. (2011) showed that O₃ and haze
89 problem had become an important issue due to the increasing of urban land-use. Liao et al. (2015)

90 further quantified the increase of O₃ and the decrease of PM₁₀ (or NO_x) related to the urban
91 expansion. Kang et al. (2014) discussed the impact of Shanghai urban land surface forcing on
92 downstream city meteorology. Zhu et al. (2015) further studied this impact on O₃ chemistry.
93 However, the above studies only took the expansion of urban land-use into account. We still need
94 to know how the excessive anthropogenic heat from urban expansion impacts on urban climate
95 and air quality. Among previous studies, a couple of researchers have tried to fill the knowledge
96 gap. For instance, He et al. (2007) incorporated AH into a PBL (planetary boundary layer) model
97 for Nanjing 2002 and found a temperature increase (0.5 - 1 °C) at night. Wang et al. (2015)
98 reported that AH can cause notable warming in almost the whole YRD, which is more significant
99 in winter than in summer. These studies only focused on the effects of AH on local meteorological
100 fields. Till now, none studies have evaluated the influence of AH on air quality over the YRD
101 region.

102 The main purpose of this study is to improve our understanding about the influence
103 mechanism of anthropogenic heat on atmospheric environment, especially in the typical polluted
104 areas of China such as the YRD region. In this paper, we focus on (1) quantifying the spatial and
105 temporal distribution of AH emissions in the YRD region, (2) implementing the gridded AH data
106 into the modified WRF/Chem model with improved AH flux parameterization, and (3) evaluating
107 the impacts of AH fluxes on meteorological condition and air quality over the YRD region.
108 Detailed descriptions about the estimating method for anthropogenic heat flux over the YRD
109 region, the adopted air quality model with configuration, and the observation data for model
110 evolution are given in Sect. 2. Main results, including the spatial and temporal distribution of AH,
111 the performance of WRF/Chem, and the exact impacts of AH on urban climate and air quality are
112 presented in Sect. 3. In the end, a summary is given in Sect. 4.

113

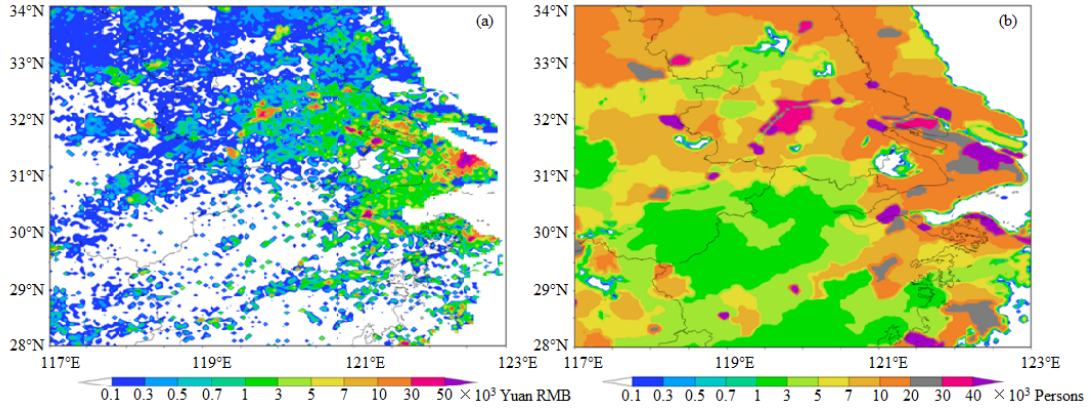
114 **2. Methodology**

115 **2.1 Anthropogenic heat flux modeling**

116 We estimate the AH fluxes during the period from 1990 to 2010 over the area between
117 (117°E, 28°N) and (123°E, 34°N), which covers the YRD region including Shanghai, southern
118 Jiangsu province and northern Zhejiang province (shown in Fig. 1). In order to get the spatial
119 distribution, this study area is also gridded as 144 rows and 144 columns with the grid spacing of

120 2.5 arcmin (approximately 4 km).

121



122

123 **Fig. 1. Spatial distribution of Gross Domestic Product (a) and population (b) in 2010 over the region**
124 **between (117°E, 28°N) and (123°E, 34°N) with the resolution of 2.5 arcmin. Data are obtained from the**
125 **website <http://sedac.ciesin.columbia.edu/gpw>.**

126

127 The anthropogenic heat flux Q_F (W/m^2) is the rate at which waste energy is discharged by
128 human activities to the surroundings (Iamarino et al., 2012). In urban areas, it usually consists of
129 the heat flux deriving from energy consumption in buildings (Q_{FB}), from the transportation sector
130 (Q_{FT}) and from human metabolism (Q_{FM}) (Grimmond 1992; Sailor and Lu, 2004; Allen et al.,
131 2011; Iamarino et al., 2012; Quah and Roth, 2012). Three general approaches have been
132 recognized to estimate these terms (Sailor, 2011), including the building energy modeling
133 approach for the building sector (Kikegawa et al., 2003), the closure of the energy budget (Offerle
134 et al., 2005), and the use of statistics on energy consumption (Sailor and Lu, 2004; Flanner, 2009;
135 Hamilton et al., 2009; Lee et al., 2009; Allen et al., 2011; Iamarino et al., 2012; Quah and Roth,
136 2012). The third method, which is also called the top-down energy inventory method, was the
137 most common approach and widely applied in AH flux predictions in China (Chen et al., 2012; Lu
138 et al., 2014; Xie et al., 2015). Based on these previous investigations, Q_F in this study is calculated
139 by the following equation:

$$140 \quad Q_F = Q_{FI} + Q_{FB} + Q_{FT} + Q_{FM} \quad (1)$$

141 where Q_{FI} represents the heat emitted from the industry sector (W/m^2).

142 According to the second law of thermodynamics, most energy used for human economy is
143 immediately dissipated as heat, other energy temporarily stored as electrical, mechanical, chemical

144 or gravitational potential energy can finally transform to high entropy thermal energy as well, and
 145 only a neglectful portion ($\ll 1\%$) might convert to radiation and escape to space (Flanner, 2009).
 146 So, it is reasonable to assume that all non-renewable primary energy consumption is dissipated
 147 thermally in Earth's atmosphere. From another perspective, in this study, the gridded AH data is
 148 finally incorporated into the single layer urban canopy model SLUCM (Kusaka and Kimura, 2004;
 149 Chen et al., 2011), in which we do not need to strictly distinguish different sources of AH. In a
 150 consequent, $Q_{F,I} + Q_{F,B} + Q_{F,T}$ at each grid can be estimated on the basis of energy consumption
 151 from non-renewable sources (coal, petroleum, natural gas, and electricity etc.) by using the
 152 following equation:

$$153 \quad Q_{F,I} + Q_{F,B} + Q_{F,T} = \eta \cdot \varepsilon_s \cdot C_s / (t \cdot A) \quad (2)$$

154 where, C_s is the primary energy consumption that has been converted to standard coal (t) at a grid.
 155 ε_s is the calorific value of standard coal (the conversion factor from primary energy consumption
 156 to heat), which is recommended to be 29271 kJ/kg in many previous studies (Chen et al., 2012; Lu
 157 et al., 2014; Xie et al., 2015). η is the efficiency of heat release in different sectors, with the typical
 158 value of 60% for electricity or heat-supply sector and 100% for other sectors (Lu et al., 2014). t is
 159 the time duration of used statistic data, and is set to be 365 (days in a year) $\times 24 \times 3600 = 31536000$
 160 s in this study. A represents the area of a grid, which is about $4 \times 4 \text{ km}^2$. To quantify the values of C_s ,
 161 the authoritative statistics of annual standard coal consumption from 1990 to 2010 in provincial
 162 level are firstly obtained from China Statistical Yearbooks and the Yearbooks in Shanghai, Jiangsu
 163 and Zhejiang. Then, the total provincial energy consumption is apportioned to each grid according
 164 to population density and converted to annual-mean gridded energy flux. The population density
 165 with the resolution of $2.5 \times 2.5 \text{ arcmin}$ in 1990, 1995, 2000, 2005 and 2010 can be downloaded
 166 from Columbia University's Socioeconomic Data and Applications Center (<http://sedac.ciesin.columbia.edu/gpw>). That for 2010 is shown in Fig. 1b for example.

168 With respect to the heat flux generated by the human metabolism ($Q_{F,M}$), the grid value is
 169 computed as:

$$170 \quad Q_{F,M} = P_g \cdot (M_d \cdot 16 + M_n \cdot 8) / 24 \quad (3)$$

171 where P_g is the population at a grid. M_d and M_n represent the average human metabolic rate
 172 (W/person) during the daytime and nighttime. 16, 8 and 24 are the hours of daytime, nighttime
 173 and a whole day, respectively. Following the previous research work (Sailor and Lu, 2004; Chen et

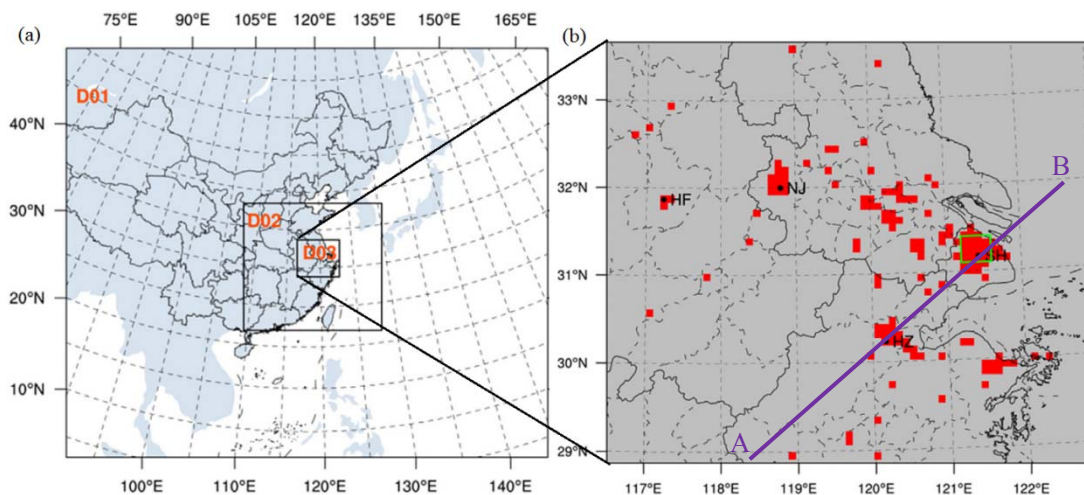
174 al., 2012; Lu et al., 2014; Xie et al., 2015), we assume that the sleeping metabolic rate M_d for a
175 typical man is 75 W, and the average daytime metabolic rate M_n in urban areas is 175 W.

176 2.2 Air quality model and configuration

177 The WRF/Chem version 3.5 is applied to investigate the impacts of AH fluxes on climate and
178 air quality over the YRD region. WRF/Chem is a new generation of air quality modeling system
179 developed at National Center for Atmospheric Research (NCAR), in which the meteorological
180 component (WRF) and the air quality component (Chem) are fully coupled using the same
181 coordinates and physical parameterizations. The feedbacks between meteorology and air
182 pollutants are included in the model. It has been proved to be a reliable tool in simulating air
183 quality from city-scale to meso-scale in China (Liu et al., 2013; Yu et al., 2014; Liao et al., 2014;
184 2015).

185 As shown in Fig. 2a, three nested domains are used in this study, with the grid spacing of 81,
186 27 and 9 km, respectively. The outermost domain (Domain 1, D01) covers most of the East Asia
187 and South Asia, the second domain (Domain 2, D02) covers central-east part of China, and the
188 finest domain (Domain 3, D03) centered at Nanjing covers the entire YRD region (Fig. 2b). For all
189 domains, from the ground level to the top pressure of 50hPa, there are 36 vertical sigma layers
190 with about 10 in the PBL. The height of the lowest level is about 25 m.

191



192

193 Fig. 2. The three nested modeling domains (a) and MODIS urban land-use category dataset used in D03,

194 with the locations of the four meteorology observation sites (b). SH, HZ, NJ and HF in (b) represent

195 Shanghai, Hangzhou, Nanjing and Hefei, respectively. Line AB denotes the location of the vertical cross

196 section used in Fig. 9 and Fig. 12.

197

198 Two simulation cases are conducted. One incorporates the urban canopy model with the
199 gridded AH fluxes that are estimated in Sect. 2.1 (referred to as ADDAH case hereafter). The other
200 only applies the same model but ignores the contribution of AH (referred to as NONAH case
201 hereafter). To exclude the uncertainty conceivably caused by different configurations, all the
202 physical schemes, chemical schemes and emission inventory are the same in both NONAH and
203 ADDAH simulations. Thus, the difference between the modeling results of NONAH and ADDAH
204 can demonstrate the impacts of anthropogenic heat. In the YRD region, January and July can be
205 representative of dry and wet season, respectively (Liao et al., 2015). Consequently, two time
206 periods are chosen for simulations and analysis. One is from 0000 UTC 01 January to 0000 UTC
207 01 February 2010, and the other is from 0000 UTC 01 July to 0000 UTC 01 August 2010, which
208 also match the time when observation data are available. **The monthly averaged difference
209 between ADDAH and NONAH can be calculated by the following algorithm:**

$$210 \quad ADDAH - NONAH = \frac{\sum_{t=1}^{744} (V_{ADDAH,t} - V_{NONAH,t})}{744} \quad (4)$$

211 where $V_{ADDAH,t}$ and $V_{NONAH,t}$ are the hourly modeling outputs of variable V (meteorological factors
212 or air pollutants) from ADDAH and NONAH, respectively. The monthly averaged differences of
213 variables are calculated grid by grid. To guarantee the differences of one variable are statistically
214 significant, student t test is carried out based on the data set from NONAH and ADDAH for each
215 grid. At one grid, if the difference is non-significant under the 95% confidence level, we can assert
216 that the AH flux cannot significantly change the meteorology or air quality at this grid (Zhuang et
217 al., 2013a; 2013b; Liao et al., 2015).

218 The detailed options for the physical and chemical parameterization schemes used in this
219 study are shown in Table 1. The major selected physical options include Purdue Lin microphysics
220 scheme, RRTM (Rapid Radiative Transfer Model) long-wave radiation scheme, Goddard
221 short-wave radiation scheme, Kain-Fritsch cumulus parameterization scheme, Noah/LSM (Land
222 Surface Model) scheme and MYJ (Mellor-Yamada-Janjic) PBL scheme. Specially, SLUCM
223 (coupled with Noah/LSM) is adopted for better simulating the urban effect on meteorological
224 conditions and pollutant distribution. The 30-sec MODIS 20 category land datasets (Fig. 2b) are

225 used to replace the default USGS (U.S. Geological Survey) land-use data, because USGS data are
 226 too outdated to illustrate the intensive land cover change over the YRD region. The default values
 227 for urban canopy parameters in SLUCM, such as building morphometry, urban fraction and
 228 roughness length etc., are replaced by the typical values in the YRD region as well, following the
 229 work of He et al. (2007) and Liao et al. (2015). The initial meteorological fields and boundary
 230 conditions (forced every 6 h) are from NCEP global reanalysis data with $1^\circ \times 1^\circ$ resolution.

231 With respect to the major chemical options, the CBM-Z gas-phase chemistry scheme and the
 232 MOSAIC aerosol scheme are chosen. CBM-Z (Carbon-Bond Mechanism version Z) contains 55
 233 prognostic species and 134 reactions (Zaveri and Peters, 1999). In MOSAIC (Model for
 234 Simulating Aerosol Interactions and Chemistry), the aerosol size distribution is divided into eight
 235 discrete size bins (Zaveri et al., 2008). Besides, aerosol direct and indirect effects through
 236 interaction with atmospheric radiation, photolysis, and microphysics routines are also taken into
 237 account in our simulations. The modeling results from the global chemistry transport model
 238 MOZART-4 are used to provide the initial chemical state and boundary conditions as described by
 239 Liao et al. (2015). The anthropogenic emissions are mainly from the inventory developed for the
 240 NASA INTEX-B mission (Zhang et al., 2009), and modified for simulations in the YRD region
 241 (Liao et al., 2014; 2105). The ammonia emission and biomass burning emissions, which are not
 242 contained in the INTEX-B inventory, are obtained from the inventory developed for TRACE-P
 243 (Streets et al., 2003). For Shanghai area, we use the additional $1 \text{ km} \times 1 \text{ km}$ source emission
 244 compiled by Shanghai Environmental Monitoring Center during EXPO 2010 (Wang et al., 2012).
 245 The biogenic emissions are estimated by using MEGAN2.04 (Guenther et al., 2006).

246

247 **Table 1. The grid settings, physics and chemistry options used in this study for WRF/Chem**

Items	Contents
Dimensions (x,y)	(85,75), (76,70), (76,70)
Grid size (km)	81, 27, 9
Time step (s)	360
Microphysics	Purdue Lin microphysics scheme (Lin et al., 1983)
Long-wave radiation	RRTM scheme (Mlawer et al., 1997)
Short-wave radiation	Goddard scheme (Kim and Wang, 2011)
Cumulus parameterization	Kain-Fritsch scheme, only for D01 and D02 (Kain, 2004)
Land surface	Noah land surface model (Chen and Dudhia, 2001)
Planetary boundary layer	Mellor-Yamada-Janjic scheme (Janjic, 1994)

Urban canopy model	SLUCM (Kusaka and Kimura, 2004)
Gas-phase chemistry	CBM-Z (Zaveri and Peters, 1999)
Aerosol module	MOSAIC using 8 sectional aerosol bins (Zaveri et al., 2008)

248

249 **2.3 Methodology for incorporating gridded AH emission data**

250 Within the Single Layer Urban Canopy Model SLUCM, the AH for each grid is determined
 251 by the fixed AH value for the urban land-use category, the fixed temporal diurnal pattern and the
 252 urban fraction value on each grid (Chen et al., 2011). AH with its diurnal variation is generally
 253 considered by adding them to the sensible heat flux from the urban canopy layer by the following
 254 equation:

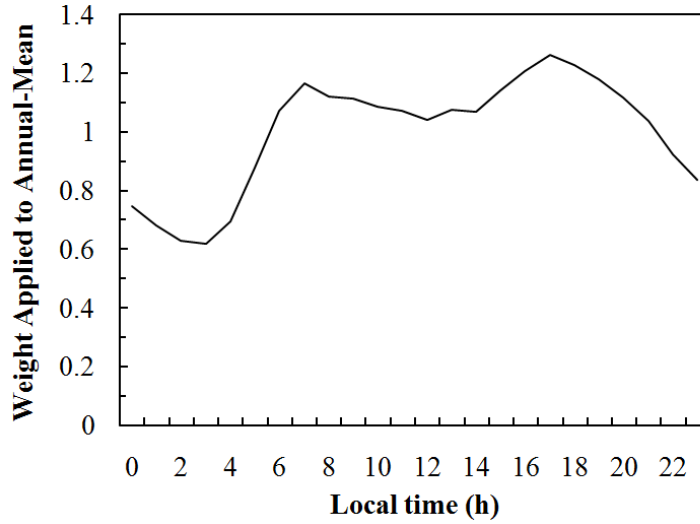
$$255 \quad Q_H = F_V \cdot Q_{HV} + F_U \cdot (Q_{HU} + Fix_{AH}) \quad (5)$$

256 where Q_H is the total sensible heat flux. F_V and F_U are the fractional coverage of natural and
 257 urban surfaces, respectively. Q_{HV} is the sensible heat flux from Noah LSM for natural surfaces,
 258 and Q_{HU} is that from SLUCM for artificial surfaces. Fix_{AH} represents the fixed AH value for all
 259 urban areas (Chen et al., 2011). In ADDAH simulation case of this study, we basically follow the
 260 Eq. 4, but incorporate the gridded AH data (Q_F) to replace the fixed AH value (Fix_{AH}) in order to
 261 considering the spatial distribution of AH fluxes. The data estimated in Sect. 2.1 with the
 262 resolution of about 4km are re-projected to domain 3 (9km) by the latitude and longitude of each
 263 grid. To account for temporal variability, the annual-mean AH fluxes in 2010 over the modeling
 264 area are further scaled with weighting functions dependent on local time of day (t_d) and time of
 265 year (m_y):

$$266 \quad Q_F(t_d, m_y) = Q_F \cdot w_d(t_d) \cdot w_y(m_y) \quad (6)$$

267 where the diurnal cycles of w_d are obtained from the work of He et al. (2007) for the YRD region
 268 (shown in Fig. 3). According to the findings of Sailor and Lu (2004) and Flanner (2009), the
 269 values of w_y for January and July are set to be 1.2 and 0.8, respectively.

270



271

272 Fig. 3 Diurnal variation of anthropogenic heat flux based on He et al. (2007), applied as weights to the
 273 annual-mean flux.

274

275 **2.4 Evaluation method and relevant observation data**

276 Meteorological and chemical observation records are used to evaluate the model performance
 277 in this study. The mean bias (MB), root mean square error (RMSE) and correlation coefficient
 278 (CORR) between observation and the ADDAH model results are used to verify model
 279 performance. In statistics, they are usually defined as:

280
$$MB = \frac{1}{N} \sum_{i=1}^N (S_i - O_i) \quad (7)$$

281
$$RMSE = \sqrt{\frac{1}{N} \sum_{i=1}^N (S_i - O_i)^2} \quad (8)$$

282
$$CORR = \frac{\sum_{i=1}^N (S_i - S_m)(O_i - O_m)}{\sqrt{\sum_{i=1}^N (S_i - S_m)^2} \sqrt{\sum_{i=1}^N (O_i - O_m)^2}} \quad (9)$$

283 where S_i is the simulation and O_i is the observation. S_m and O_m are average value of simulations
 284 and observations, respectively. In general, the model performance is acceptable if the values of
 285 MB and RMSE are close to zero and those of CORR are close to 1.

286 With respect to observed meteorological data, four observation sites are selected, which are
 287 NJ (32.00°N, 118.80°E) located in Nanjing, HF (31.87°N, 117.23°E) in Hefei, HZ (30.23°N,
 288 120.16°E) in Hangzhou, and SH (31.40°N, 121.46°E) in Shanghai, respectively (marked in Fig.

289 2b). Their time series of 2-m temperature, 10-m wind speed and 2-m relative humidity in January
290 and July of 2010 can be obtained from hourly records of atmospheric sounding dataset compiled
291 by University of Wyoming (<http://weather.uwyo.edu>). In order to evaluate model performance of
292 chemical fields, hourly chemical series of PM₁₀ and O₃ during the modeling period are acquired
293 from Caochangmen (CCM) site. CCM is located in the central and highly residential area of
294 Nanjing (32.06°N, 118.74°E), and is running by the Nanjing Environmental Monitoring Center.
295 The assurance/quality control (QA/QC) procedures at CCM strictly follow the national standards.

296

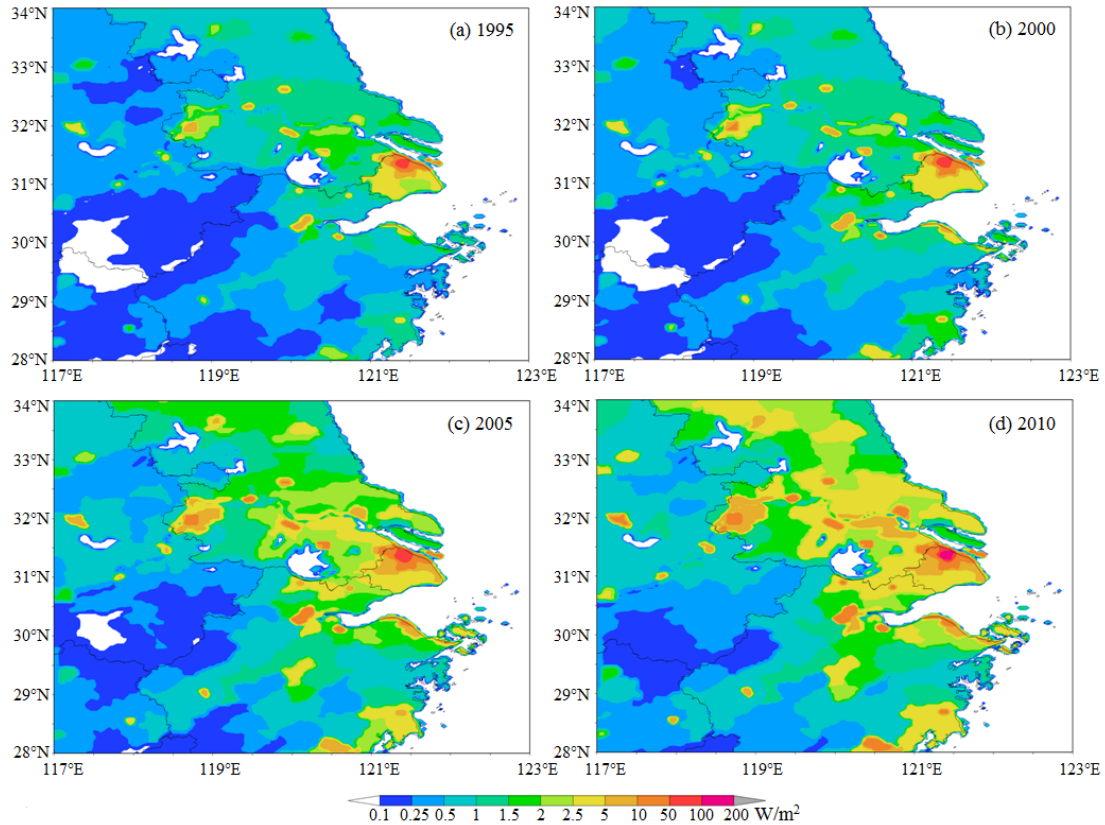
297 **3. Results and discussions**

298 **3.1 Spatial and temporal distribution of anthropogenic heat flux in the YRD region**

299 Using the methodology outlined above in Sect. 2.1, we construct the spatial distribution of
300 anthropogenic heat fluxes over the YRD region from 1990 to 2010 with a 5-year interval. Fig. 4
301 illustrates the gridded distribution in 1995, 2000, 2005 and 2010 (The magnitude and spatial
302 distribution pattern in 1990 are similar to 1995). Obviously, big cities, such as Shanghai, Nanjing,
303 Hangzhou etc., have the largest values among neighboring areas from the early 1990s till now.
304 Before 2000, except for some megacities, AH fluxes are generally less than 2.5 W/m² in most
305 parts of the YRD region. However after 2000, the AH fluxes are more than 5 W/m² in many areas,
306 with the high values over 25 W/m² centrally appearing along the Yangtze River, around Lake
307 Taihu and beside Hangzhou Bay. The temporal variation of the spatial pattern fits in well with the
308 economic boom in the YRD region over the past decades.

309 Being the largest city, Shanghai always has the highest anthropogenic heat emissions in the
310 YRD region. As shown in Table 2, the annual mean value over the whole administrative district is
311 5.47 W/m² in 1990 and 14.45 W/m² in 2010, with the annual growth of 0.45 W/m². In recent years,
312 the AH fluxes in the city center of Shanghai have exceeded 100 W/m², which is comparable to
313 those in the most crowded megacities, such as Tokyo (Ichinose et al., 1999), Hong Kong (Flanner,
314 2009), London (Hamilton et al. 2009; Iamarino et al. 2012) and Singapore (Quah and Roth, 2012).
315 The annual mean values in the downtown area are much higher than the regional ones. With
316 respect to Jiangsu Province and Zhejiang Province, the AH fluxes there also increase from 0.68
317 and 0.33 W/m² in 1990 to 2.61 and 1.63 W/m² in 2010. The regional annual mean values in
318 Jiangsu higher than those in Zhejiang can be attributed to the facts that there are more large

319 state-owned enterprises (including petrochemical companies and power plants) in Jiangsu.
 320 Furthermore, the AH fluxes in the urban areas of Jiangsu and Zhejiang range from 20 to 50 W/m²
 321 in recent decade. These high values are close to those in Toulouse of France (Pigeon et al., 2007),
 322 Seoul of Korea (Lee et al., 2009), and some large US cities (Sailor and Lu, 2004; Fan and Sailor,
 323 2005).
 324



325
 326 **Fig. 4. Estimates of annual-mean anthropogenic heat fluxes resulting from the consumption of**
 327 **non-renewable energy sources (coal, petroleum, natural gas, and electricity) and human metabolism**
 328 **between (117°E, 28°N) and (123°E, 34°N) with the resolution of 2.5 arcmin for 1995 (a), 2000 (b), 2005 (c)**
 329 **and 2010 (d), respectively.**

330

331 **Table 2 The statistics of annual average anthropogenic heat flux in different administrative district over the**
 332 **YRD region (W/m²)**

Province or Municipality		This study					Previous results (year)	References
		1990	1995	2000	2005	2010		
Shanghai	Regional	5.47	7.85	9.2	12.39	14.45	16.54 (2008)	Chen et al., 2012
	Downtown	42	60.8	71.6	96.9	113.5	117.7 (2010)	Lu et al., 2014
Jiangsu	Regional	0.68	0.94	0.99	1.83	2.61	2.32 (2008)	Chen et al., 2012
	Downtown	5.1	9.5	12.5	28.6	50.2	40 (Nanjing, 2007)	He et al., 2007

							20-70 (2010)	Lu et al., 2014
	Regional	0.33	0.54	0.73	1.25	1.63	1.60 (2008)	Chen et al., 2012
Zhejiang	Downtown	2.7	7.4	12.1	25.1	39.3	50 (Hangzhou, 2007)	He et al., 2007
							20-70 (2010)	Lu et al., 2014

333 * Regional represents the average value over the whole area of an administrative district, while Downtown
 334 represents the high value in the city center.

335

336 In 2010, nearly all areas of the YRD region have the AH fluxes more than 2.5 W/m² (shown
 337 in Fig. 4d). **High** fluxes generally occur in and around the cities, such as Shanghai, Nanjing,
 338 Hangzhou, Yangzhou, Zhenjiang, Taizhou, Changzhou, Wuxi, Suzhou, Nantong, Huzhou, Jiaxing,
 339 Shaoxing, and Ningbo etc., with the typical values of 113.5, 50.2 and 39.3 W/m² in the urban areas
 340 of Shanghai, Jiangsu and Zhejiang, respectively (shown in Table 2). Comparing Fig. 4d with Fig.
 341 1, we can easily find that the spatial distribution of AH based on the population reflects the
 342 economic activities in the YRD region as well, suggesting that our method is effective and the
 343 results are reasonable. Moreover, as shown in Table 2, parts of our conclusion can be supported by
 344 some other previous studies (He et al., 2007; Chen et al., 2012; Lu et al., 2014; Xie et al., 2015).
 345 Therefore, the gridded AH fluxes can be used in meso-scale meteorological and environmental
 346 modeling to investigate their impacts on urban climate and air quality.

347

348 3.2 Model evaluation for WRF/Chem

349 Table 3 shows the statistical comparisons between meteorological observations and the
 350 model results from both January and July simulations in ADDAH case. Mean values, MB, RMSE
 351 and CORR are all quantified for 2-m temperature (T₂), 2-m relative humidity (RH₂) and 10-m
 352 wind speed (WS₁₀) at four grids where NJ, HF, HZ and SH are located. As shown in Table 3, the
 353 correlation coefficients between observations and simulations (CORR) are over 0.9 in January and
 354 about 0.8 in July for T₂, **higher** than 0.7 for RH₂ at most sites in both months, and close to 0.7 for
 355 WS₁₀ in January. So WRF/Chem simulates the urban meteorological conditions over the YRD
 356 region quite well. With respect to T₂, the modeling results are slightly overvalued at all sites,
 357 which might be attributed to the uncertainty caused by urban canopy and surface parameters
 358 (Kusaka and Kimura, 2004; Chen et al., 2011; Liao et al., 2015). But the level of overestimation is
 359 acceptable, because the MB values of T₂ are only 1.1 - 1.7 °C in January and 0.7 - 2.0 °C in July

360 with the RMSE of T_2 are 1.6 - 2.2 °C. The lowest value 0.7 °C for MB and the highest value 0.94
361 for CORR illustrate the best T_2 estimation at SH. For RH_2 , compared with the observations, the
362 simulation results are underestimated at all sites. Though worst simulation of RH_2 occurs at HF,
363 the results are reasonable at other three sites. We find that the land-use dataset cannot well
364 describe waters around HF. In view that HF is not in the center area of the YRD region, the
365 deviation at HF cannot introduce crucial uncertainty into our main conclusion. In regard to WS_{10} ,
366 the modeling values from the ADDAH case are slightly overestimated at NJ, HF and HZ, whereas
367 underestimated at SH. The MB for WS_{10} is generally less than 0.5 m/s, and the RMSE is less than
368 1.3 m/s. These over- or under-estimates are attributable to near-surface wind speed being
369 influenced by local underlying surface characteristics more than other meteorological parameters.
370 Further improvement of urban canopy parameters might improve the simulations (Zhang et al.,
371 2010; Liao et al., 2015).

372

373 **Table 3 The statistics of meteorological conditions from the ADDAH simulation at four sites**

Vars ^a	Sites ^b	January					July				
		Mean ^c		MB	RMSE	CORR ^d	Mean ^c		MB	RMSE	CORR ^d
		OBS ^e	SIM ^f				OBS ^e	SIM ^f			
T_2 (°C)	NJ	3.5	5.1	1.6	2.2	0.92	28.2	30.2	2.0	2.0	0.83
	HZ	5.7	7.4	1.7	1.9	0.93	28.7	30.5	1.8	2.2	0.80
	HF	3.6	5.1	1.5	2.2	0.91	28.9	30.6	1.7	2.1	0.76
	SH	5.6	6.7	1.1	1.6	0.94	28.8	29.5	0.7	1.7	0.85
RH_2 (%)	NJ	65	53	-12	14	0.74	76	68	-9	10	0.71
	HZ	67	60	-7	10	0.83	74	70	-4	17	0.71
	HF	71	51	-20	13	0.75	88	69	-19	12	0.62
	SH	70	64	-6	11	0.79	76	72	-4	11	0.77
WS_{10} (m/s)	NJ	2.6	3.1	0.5	1.2	0.61	2.9	3.2	0.3	1.3	0.53
	HZ	2.5	2.6	0.1	1.0	0.69	2.4	2.5	0.1	1.3	0.34
	HF	2.6	2.9	0.3	1.1	0.67	2.3	2.7	0.4	1.2	0.40
	SH	4.1	3.8	-0.3	1.2	0.78	4.1	3.6	-0.5	1.2	0.66

374 ^a Vars represents the variables, including temperature at 2m (T_2), relative humidity at 2m (RH_2) and wind speed at
375 10m (WS_{10}).

376 ^b Sites indicates the observation meteorological sites used in this study, including NJ in Nanjing, HF in Hefei, HZ
377 in Hangzhou and SH in Shanghai.

378 ^c Mean represents the average value.

379 ^d CORR indicates the correlation coefficients, with statistically significant at 95% confident level.

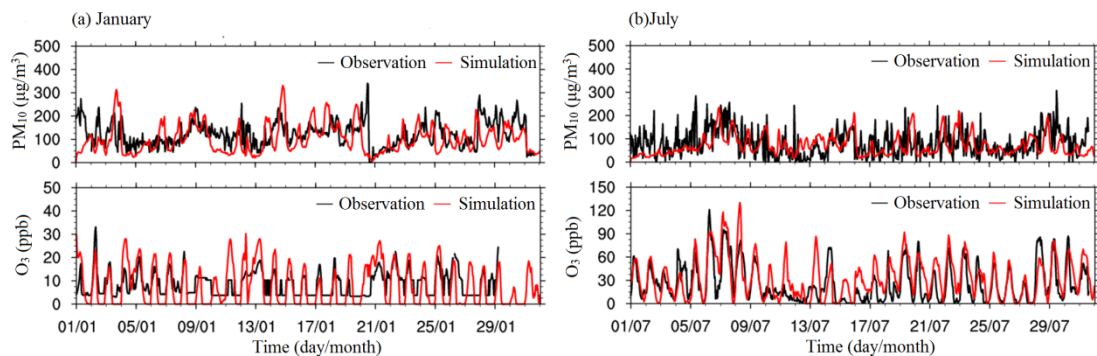
380 ^e OBS represents the observation data.

381 ^f SIM indicates the simulation results from WRF/Chem.

382

383 Fig. 5 presents time series comparisons between the observation data of O₃ and PM₁₀ at CCM
384 and their modeling results from the ADDAH simulation case. Obviously, WRF/Chem with
385 gridded AH fluxes can capture diurnal variations and magnitude of these pollutants. For O₃, the
386 correlation coefficient between observations and simulations (CORR) is 0.60 in January and 0.71
387 in July (statistically significant at 95% confident level). The value of MB is -0.8 ppb in January
388 and 7.0 ppb in July, which can be explained that stronger solar radiation reaches to urban surface
389 in July causing positive biases in T₂, and thereby produces more O₃ within PBL (Zhang et al.,
390 2010; Liao et al., 2015). In regard to PM₁₀, the model prediction underestimates the concentration
391 with MB being -19.9 μg/m³ in January and -10.8 μg/m³ in July respectively. This underestimate
392 can be partially ascribed to positive biases of T₂, which induce an increase of PBL height and
393 cause PM₁₀ diluting within PBL (Liao et al., 2015). Furthermore, uncertainties in emissions may
394 also cause these biases.

395



396

397 **Fig. 5. Hourly variations of PM₁₀ (μg/m³) and O₃ (ppb) from the observation data and the ADDAH**
398 **simulation results at CCM monitoring site in Nanjing for January (a) and July (b).**

399

400 Liao et al. (2014) also simulated the same time periods in the YRD region by running
401 WRF/Chem with a fixed AH flux in SLUCM. They found that the default SLUCM scheme tends
402 to underestimate 2-m temperature in January but overestimate it in July, and overestimate the wind
403 speed in both months. In a consequent, their chemical predictions are not so perfect as well, with
404 the CORR of 0.44-0.52 for O₃ and 0.19-0.33 for PM₁₀. Compared with their results, our
405 simulations accounting for the temporal and spatial distribution of AH improve the accuracy of the
406 model results, and well predict the urban climate and air quality.

407 Generally, the WRF/Chem with gridded AH fluxes has relatively good capability on
408 simulating urban climate and air quality over the YRD region in this study. Though the biases are
409 still found, the difference between the modeling results from NONAH and ADDAH can still
410 quantify the impacts of anthropogenic heat on meteorology and pollution, because all other
411 conditions are the same in both simulations.

412

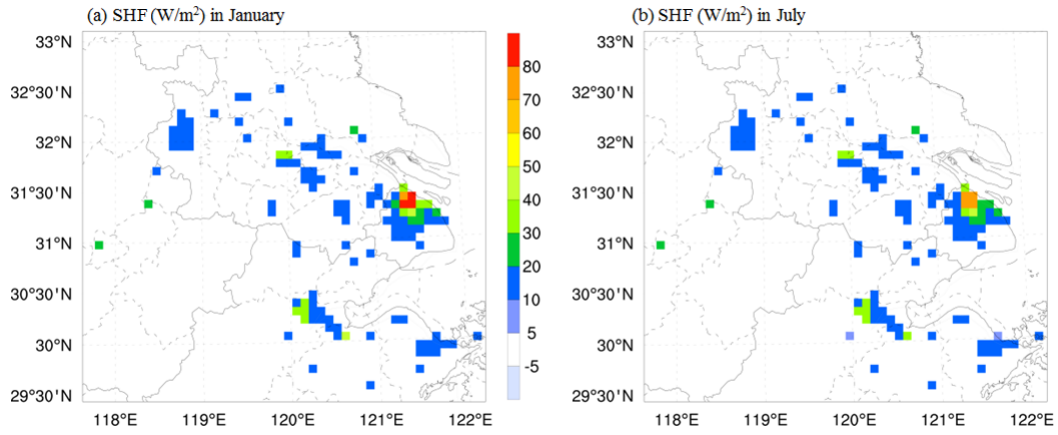
413 3.3 Impacts of AH on meteorological conditions

414 3.3.1 Horizontal meteorology changes

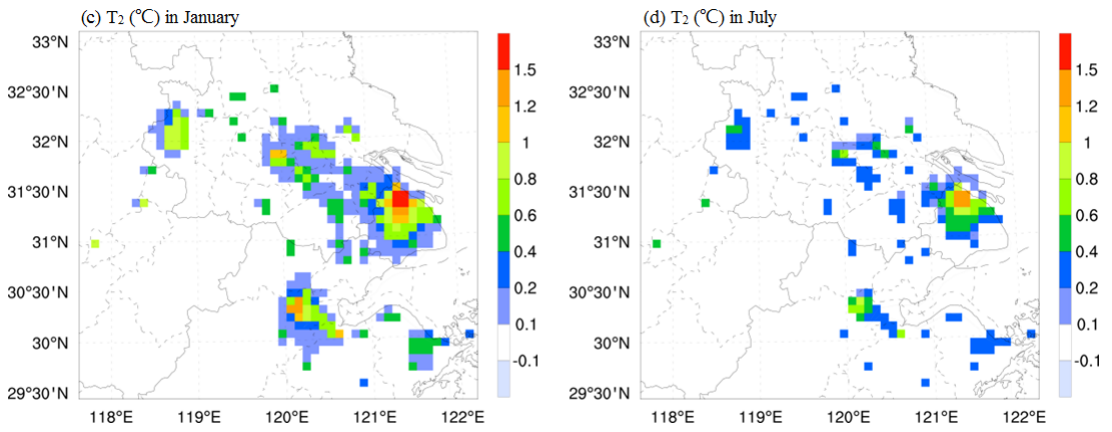
415 Fig. 6 presents the monthly-averaged differences of main meteorological factors between
416 ADDAH and NONAH (ADDAH-NONAH) over the modeling domain 3 (D03). Differences that
417 are non-significant under the 95% confidence level using student t-test have been masked out.
418 Obviously, the emissions of anthropogenic heat increase the sensible heat fluxes from the urban
419 canopy layer over the YRD region. As shown in Fig. 6a and b, the spatial patterns of sensible heat
420 changes in both January and July are similar to the spatial distribution of AH fluxes (Fig. 4d).
421 High values of variation ($> 10 \text{ W/m}^2$) generally occur around mega-cities with a positive
422 magnitude. For instance, in Shanghai, due to the maximum AH fluxes in the city center, the
423 biggest increase of sensible heat flux for January can be 82 W/m^2 , and the value is 75 W/m^2 in
424 July. In other cities, such as Hangzhou, Changzhou and Nantong etc., high values over 20 W/m^2
425 can be found in both months as well. In order to better understand the different behavior during
426 the daytime and at night, the monthly-averaged diurnal variations of these modeled meteorological
427 factors over the urban area of Shanghai in January and July are also calculated. As illustrated in
428 Fig. 7, the addition AH fluxes lead to an obvious increase of sensible heat flux (SHF) from 07:00
429 to 21:00, with the daily mean increase of 22 W/m^2 for January and 20.5 W/m^2 for July. The
430 increases are insignificant at night because the AH fluxes are small during these time. On account
431 that AH and its diurnal variation are only added to the sensible heat item, there are no significant
432 differences between the ADDAH and the NONAH simulation for ground heat flux (GRDFLX)
433 and latent heat flux (LH). It is worth mentioning that many AH emission processes are related to
434 water vapor releasing, and thereby latent heat fluxes might be affected by the human activities that
435 release AH.

436

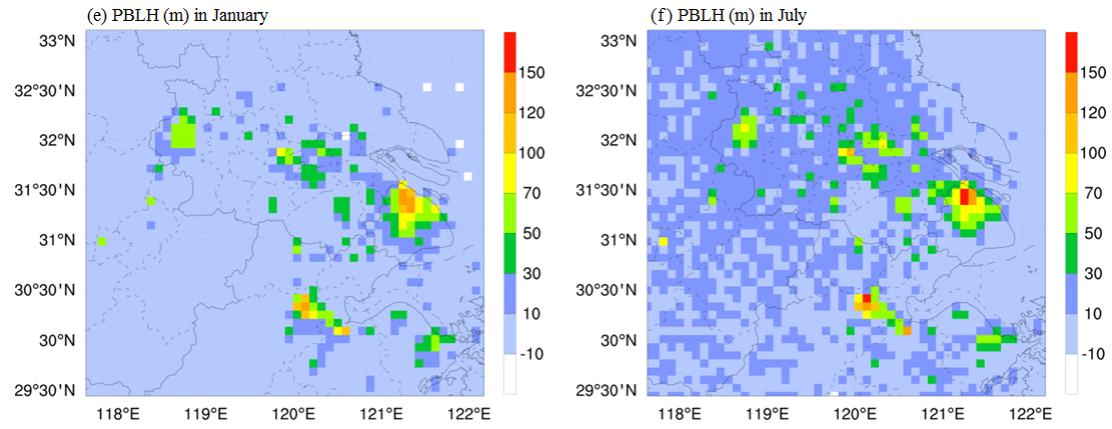
437



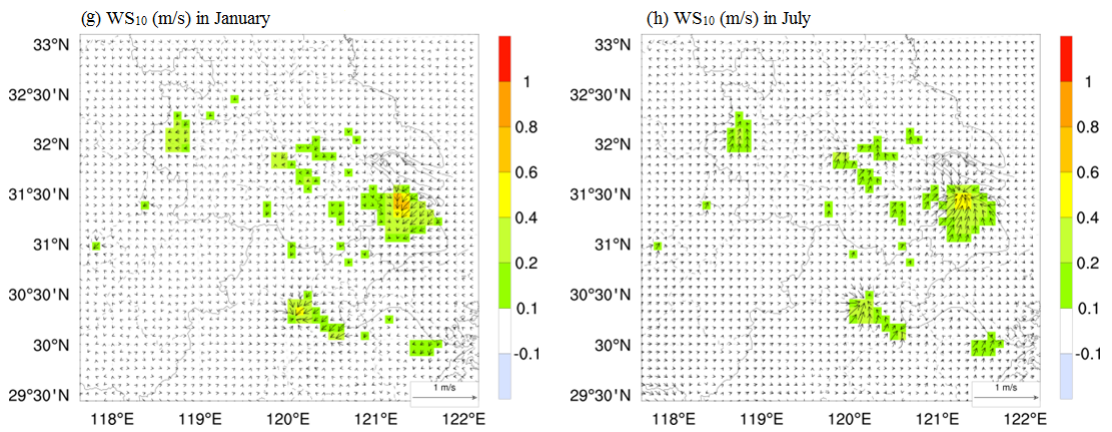
438



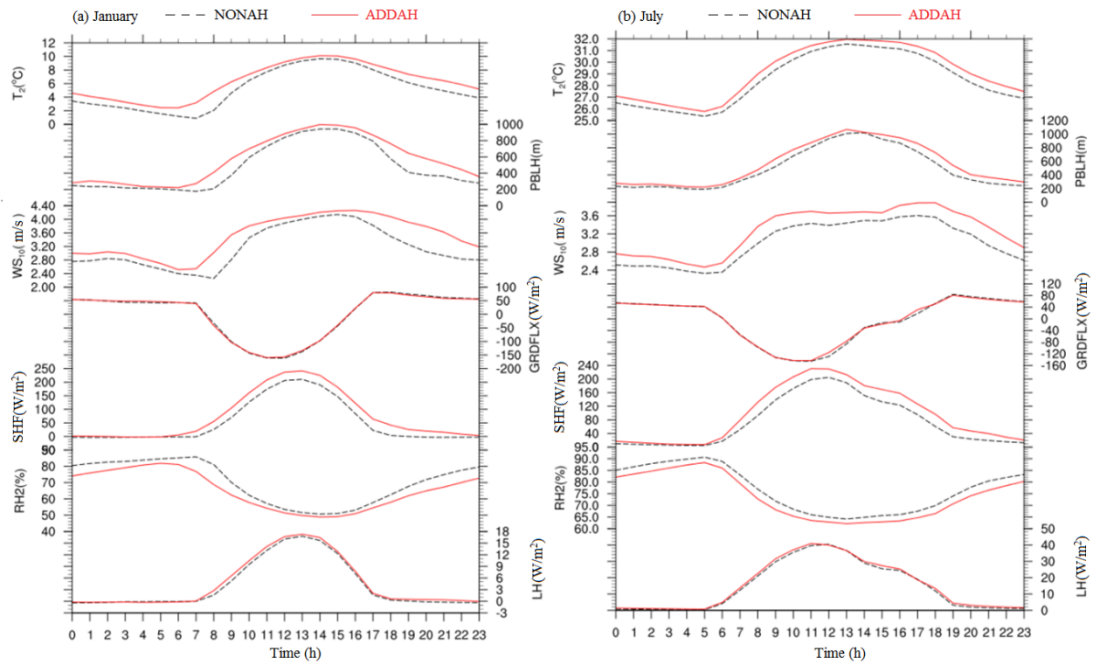
439



440



441 Fig. 6. The spatial distributions of monthly-averaged differences for sensible heat flux (SHF), air
 442 temperature at 2 m (T_2), the height of planetary boundary layer (PBLH), and wind speed (WS_{10}) at 10 m
 443 between ADDAH and NONAH (ADDAH-NONAH). (a), (c), (e) and (g) show changes in January. (b), (d), (f)
 444 and (h) illustrate variations in July. The arrows in (g) and (h) are the differences of wind fields. Differences
 445 that are non-significant under the 95% confidence level (student t-test) are masked out.
 446



447
 448 Fig.7. The monthly-averaged diurnal variations of modeled meteorological factors in January (a) and July
 449 (b) over the urban area of Shanghai. NONAH and ADDAH represent the simulation cases with and without
 450 AH fluxes, respectively. LH means latent heat. SHF indicates sensible heat flux. GRDFLX represents heat
 451 flux from ground level. T_2 , RH2, WS_{10} , and PBLH indicate 2-m air temperature ($^{\circ}\text{C}$), 2-m relative humidity
 452 (%), 10-m wind speed (m/s) and the height of planetary boundary layer (m), respectively.
 453

454 By adding more surface sensible heat into the atmosphere, the AH flux changes can influence
 455 the 2-m air temperature (T_2) as well. The patterns of the monthly-averaged T_2 changes (Fig. 6c
 456 and d) are similar to those of SHF (Fig. 6a and b). For city centers like Shanghai, Hangzhou and
 457 Nanjing, adding AH can lead to the increase of T_2 over 1°C in January and over 0.5°C in July,
 458 generating an enhanced Urban Heat Island. The maximum T_2 changes usually occur in the city
 459 center of Shanghai, with the typical value of 1.6°C in January and 1.4°C in July. These findings
 460 are comparable to the values estimated in megacities all over the world (Fan and Sailor, 2005;

461 Ferguson and Woodbury, 2007; Chen et al., 2009; Zhu et al., 2010; Menberg et al., 2013; Wu and
462 Yang, 2013; Bohnenstengel et al., 2014; Feng et al., 2014; Yu et al., 2014). Moreover, the mean
463 increase of T_2 at night in January (1.2°C) is larger than that in the daytime (1.0°C), whereas the
464 increase during the daytime and nighttime is all equal to 0.6°C in July, suggesting that AH can
465 help to form a weakened diurnal T_2 variation in winter.

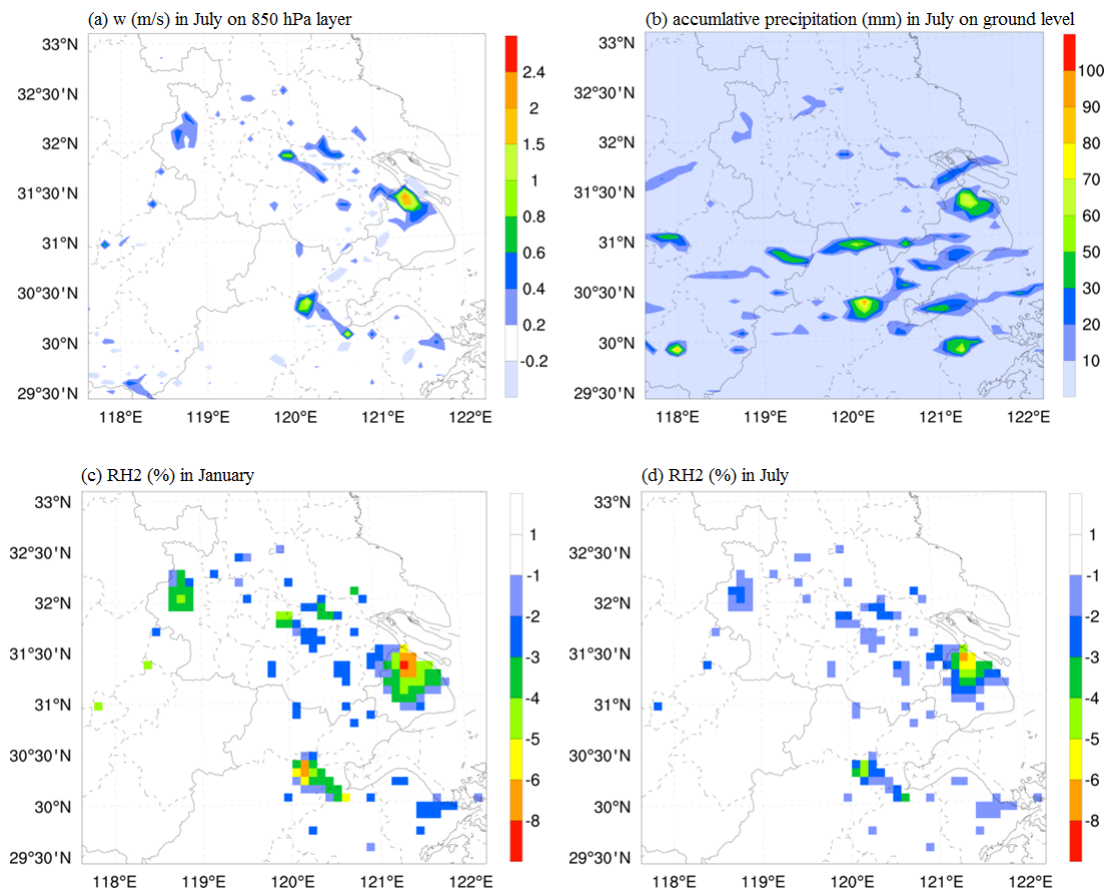
466 The vertical air movement in PBL can be enhanced by the warming up of surface air
467 temperature, which might increase the height of PBL (PBLH). Consequently, **the enhanced AH**
468 **fluxes increase the PBLH by more than 50m** in January and more than 70m in July over the YRD
469 urban areas, with the maximum changes (140m for January and 160m for July) occurring in
470 Shanghai (shown in Fig. 6e and f). **In summer, the weather is more unstable and the vertical**
471 **convection is easy to form. So the adding AH induces more increase of PBLH in July. For both**
472 months, as shown in Fig. 7, the daytime relative increase of PBLH (10%-15%) is smaller than that
473 at night (23% - 33%), which can be attributed to the facts that the absolute PBLH values are lower
474 and the air temperature increases more during the nighttime.

475 Fig. 6g and h show the changes in wind components over the YRD region, and demonstrate
476 that AH can enhance the 10-m wind speed (WS_{10}) in the urban areas. The maximum increase is
477 located in Shanghai, with the increment of 0.7 m/s (19%) in January and 0.5 m/s (17%) in July. In
478 other cities like Hangzhou and Nanjing, the added value is only about 0.3 m/s. Over the YRD
479 region, increase of WS_{10} is more obvious in January (Fig. 6g) than in July (Fig. 6h), and is slightly
480 higher at night than in daytime (Fig. 7). As mentioned in previous studies, the above increase of
481 wind speed can be ascribed to the strengthened urban-breeze circulation caused by **the enhanced**
482 **AH fluxes** (Chen et al., 2009; Ryu et al., 2013; Yu et al., 2014), which can be further clarified
483 by the surface stronger convergence wind patterns occurring around the megacities shown in Fig.
484 6g and h. The simulated divergence at the surface near cities decreases 0.07-0.23 /s in January and
485 0.08-0.31 /s in July (not shown), also providing further evidence that the convergence is enhanced
486 in these areas.

487 The strengthened urban-breeze circulation caused by adding AH can also enhance the
488 vertical movement of atmosphere. As shown in Fig. 8a, the simulated vertical velocity above the
489 megacities on 850 hPa layer increases about 2 cm/s in July, suggesting that the convection
490 movements that can transport moisture and pollutants from surface to upper layer are strengthened

491 in the urban areas. Thus, the spatial and vertical distributions of moisture are **modified**. Fig. 8c and
 492 d illustrate the spatial plots for monthly-averaged differences of 2-m relative humidity (RH₂)
 493 caused by adding AH (ADDAH-NONAH). The negative centers over the cities (the AH centers)
 494 can be seen in both January (-2 to -8%) and July (-2 to -6%), meaning the air near the surface
 495 became dryer. More moisture transported into the mid-troposphere (the vertical profile is
 496 discussed in Fig. 9g and h in details) might enhance rainfall inside urban areas as well. As shown
 497 in Fig. 8b, the increase of rainfall in July can be 72.4, 84.6 and 63.2 mm in Shanghai, Hangzhou
 498 and Ningbo, respectively. However, because of the negligible accumulative precipitation in winter,
 499 the increment of rainfall over the YRD region in January **can be ignored** (not shown).

500



501

502

503 **Fig. 8. The spatial distributions of monthly-averaged differences for 2-m relative humidity (RH₂), surface**
 504 **accumulative precipitation and vertical wind velocity on 850 hPa layer (w) between ADDAH and NONAH**
 505 **(ADDAH-NONAH). Differences that are non-significant under the 95% confidence level (student t-test) are**
 506 **masked out**

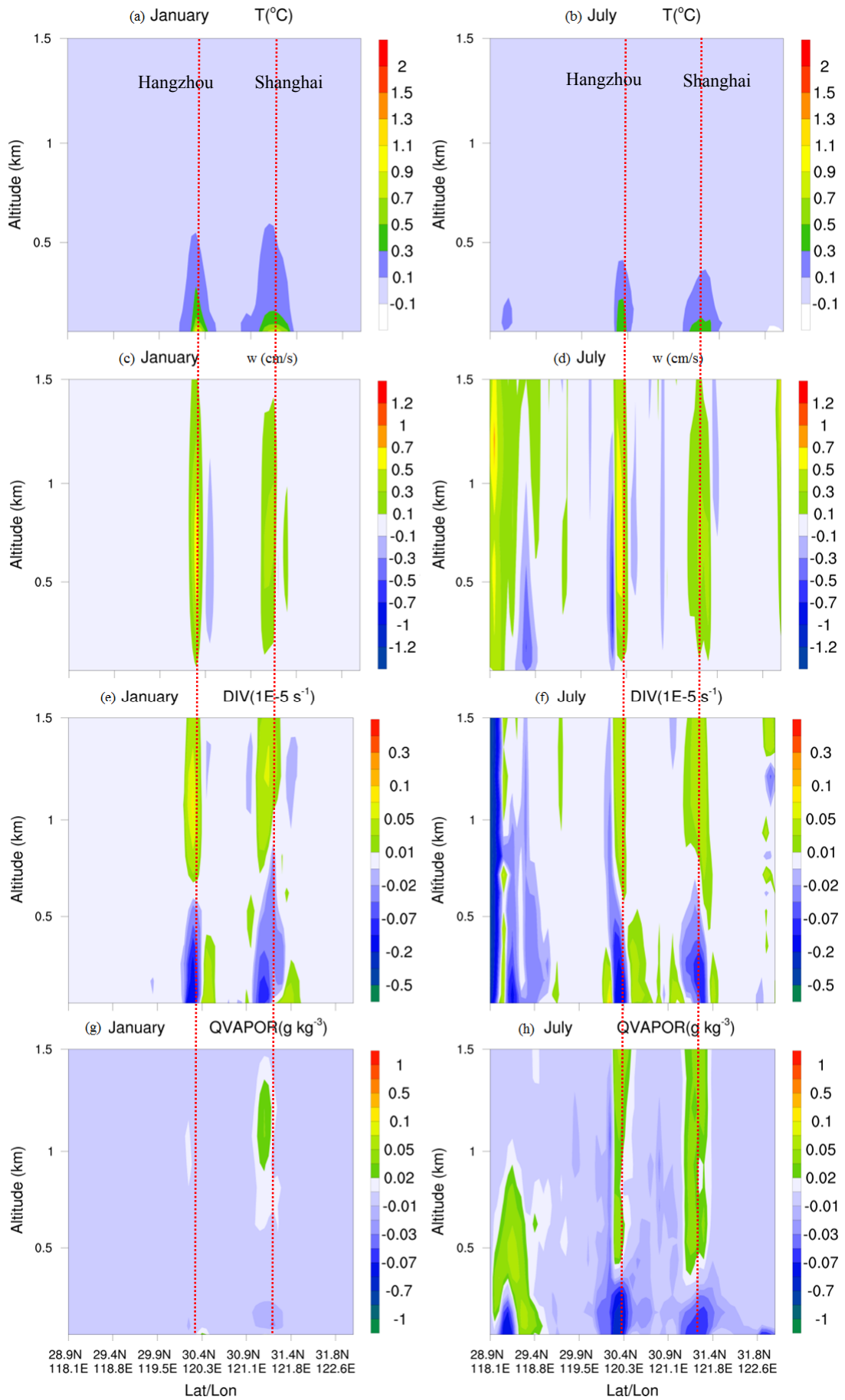
507

508 3.3.2 Vertical meteorology changes

509 To better understand how AH change the vertical and spatial distribution of meteorology in
510 the YRD region, we present changes (ADDAH - NONAH) of air temperature (T), vertical wind
511 velocity (w), divergence (DIV) and water vapor mixing ratio (QVAPOR) along a cross-section
512 from (28.9°N, 118.1°E) to (31.8°N, 122.6°E) as shown by the solid line AB in Fig. 2b. The
513 vertical cross sections for T changes (Fig. 9a and b) illustrate that adding AH leads to a significant
514 increase in air temperature near the surface around the cities (Shanghai and Hangzhou), while the
515 changes are close to 0 in the rural areas and free troposphere. The monthly mean increment of T
516 over Shanghai and Hangzhou at ground level in January (0.7°C) is bigger than that in July (0.4°C),
517 which can be attributed to the facts that the relative increase of heat is higher in January due to
518 background heat fluxes are much lower in winter.

519 The warming of air temperature near surface in cities, as well as the rising of PBLH in these
520 areas (Fig. 6e and f), can generate an enhanced urban heat island. As shown in Fig. 9c and d, the
521 vertical wind velocities above Shanghai and Hangzhou increase with added values of 0.3 – 0.7
522 cm/s in both months, whereas w in the rural areas decreases about -0.3m/s in January and -0.5
523 cm/s in July, suggesting that there are an enhanced upward movement in cities and an enhanced
524 downward movement in countryside. We also analyze the divergence changes along the
525 cross-section including Shanghai and Hangzhou (Fig. 9e and f). It can be seen that adding AH
526 decreases DIV from surface to 750m and increases DIV at higher levels, which means that there is
527 a stronger convergence wind pattern in lower PBL and a more divergent wind pattern in higher
528 PBL. This changing implies that the atmosphere is more unstable, and intends to promote the
529 development of deep convection in troposphere. Consequently, impacted by the strengthened
530 urban-breeze circulation, more moisture is transported from surface to the upper levels (over 1km),
531 with 0.6g/kg decrease of QVAPOR at the ground level and 0.1g/kg increase for the upper PBL in
532 July as presented in Fig. 9g and h. Furthermore, the abovementioned vertical changes of w, DIV
533 and QVAPOR are only restricted to the air column over the AH emission centers (Shanghai and
534 Hangzhou) in January, while the changes distribute widely (the adding AH fluxes can impact
535 wider areas) in July. This seasonal difference can be ascribed to the facts that the atmosphere is
536 more stagnant in winter and more convective in summer.

537



539 Fig. 9 The vertical distribution of monthly-averaged differences for air temperature (T), vertical wind
540 velocity (w), divergence (DIV), and water vapor mixing ratio (QVAPOR) between ADDAH and NONAH
541 (ADDAH-NONAH) from surface to 1.5km altitude along the line AB (shown in Fig. 2b). (a), (c), (e) and (g)
542 show changes in January. (b), (d), (f) and (h) illustrate variations in July. Differences that are
543 non-significant under the 95% confidence level (student t-test) are masked out.

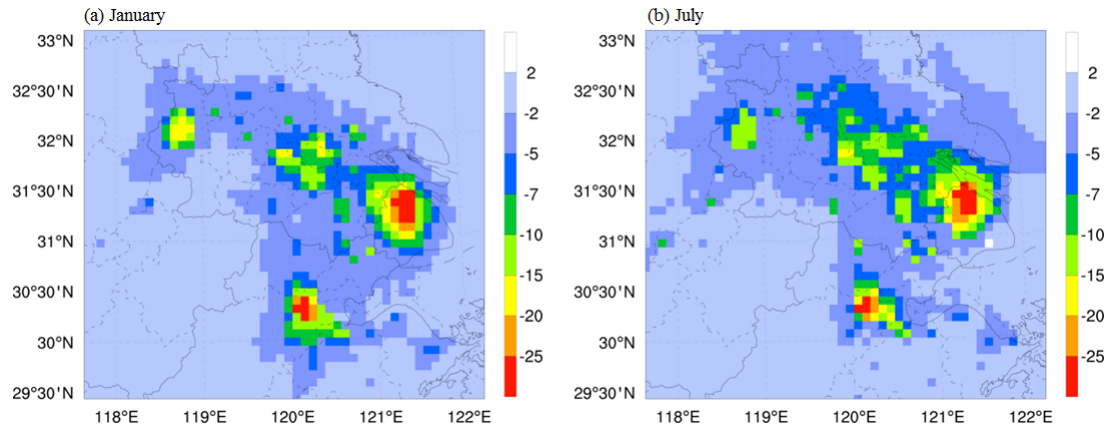
544

545 3.4 Impacts of AH on air pollutants

546 3.4.1 Changes of surface PM₁₀ and O₃

547 Adding AH changes spatial and vertical meteorology conditions, and thereby undoubtedly
548 affects the transportation and dispersion of air pollutants. Due to PM₁₀ is the main pollutant in
549 YRD region (Wang et al., 2012; Xie et al., 2014; Liao et al., 2015), it is chosen as an indicator to
550 show the changes of primary air pollutants in this study. Fig. 10 illustrates the influence of AH on
551 PM₁₀ spatial distribution in typical months of winter and summer (differences that are
552 non-significant at 95% confidence level using t-test are masked out). Results show that PM₁₀ in
553 the lowest modeling layer is reduced at all times around the cities, especially in Shanghai, Nanjing
554 and Hangzhou. The maximum decrease usually appears in Shanghai, with the monthly mean
555 reduction of 29.3 $\mu\text{g}/\text{m}^3$ (24.5%) in January and 26.6 $\mu\text{g}/\text{m}^3$ (18.8%) in July. Compared with the
556 distribution of AH emissions (Fig. 4) and meteorology changes (Fig. 6), the reduction in surface
557 PM₁₀ should be mainly related with the increase in PBLH, the rising up of surface wind speed and
558 the enhanced upward movement of air, because these modifications of meteorological conditions
559 caused by adding AH over the urban areas can facilitate PM₁₀ transport and dispersion within the
560 urban boundary layer. Furthermore, on account that the precipitation around the cities increases by
561 15-30%, the wet scavenging can contribute to the reductions of the surface PM₁₀ concentrations as
562 well.

563



564

565 **Fig. 10** The spatial distributions of monthly-averaged differences for PM_{10} between ADDAH and NONAH
 566 (ADDAH-NONAH). Differences that are non-significant under the 95% confidence level (student t-test) are
 567 masked out.

568

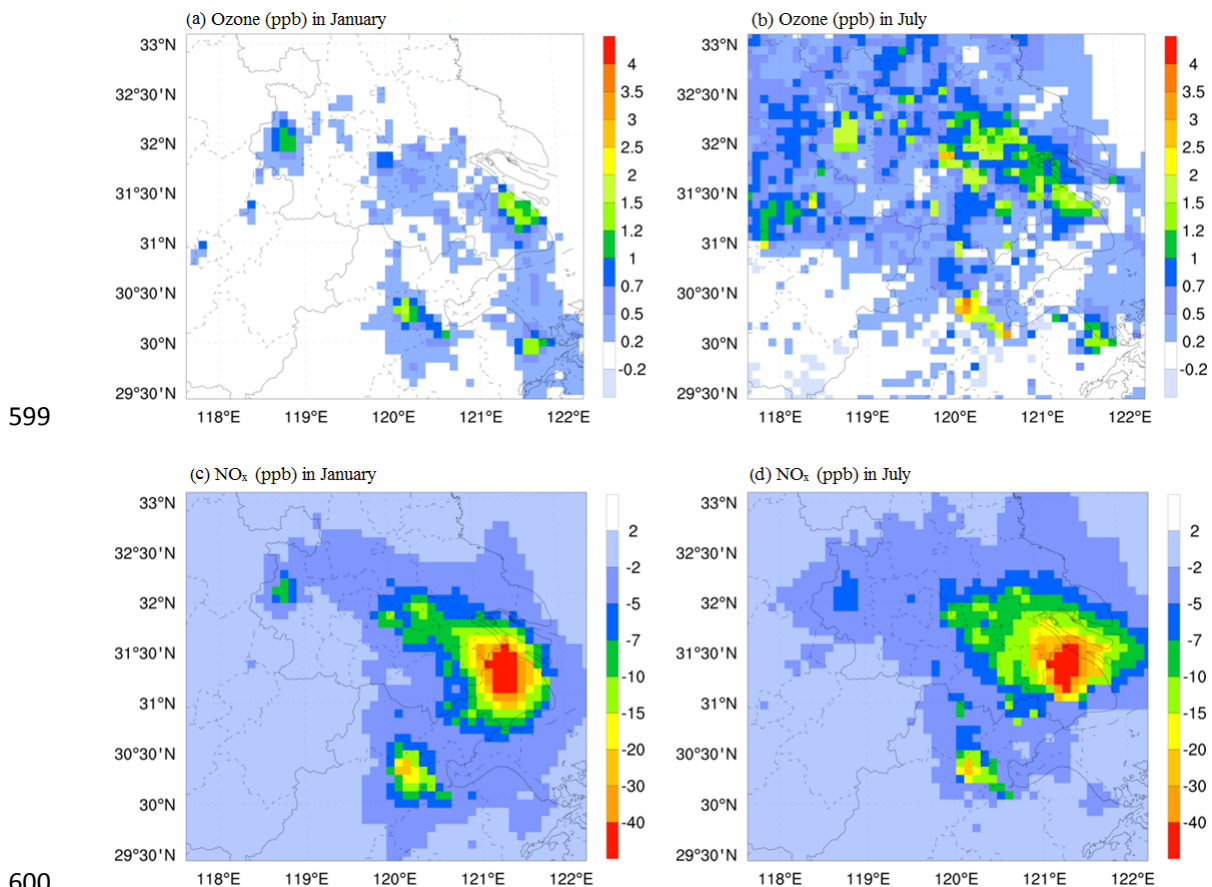
569 Spatial distribution of O_3 concentration can also be influenced by the changes of
 570 meteorological conditions due to adding AH. It should be noted that the increase of wind speed
 571 might facilitate O_3 transport, and the rising up of PBLH can lead to O_3 dilution within planetary
 572 boundary layer. Thus, the surface O_3 concentrations are seemingly reduced. However, unlike PM_{10} ,
 573 O_3 is a secondary air pollutant formed by a series of complex chemical reactions involving oxides
 574 of nitrogen ($NO_x=NO+NO_2$) and volatile organic compounds (VOCs), so only considering the
 575 factors affecting O_3 transport and dispersion is not sufficient. In fact, O_3 changes are different
 576 from those of PM_{10} . As illustrated in Fig. 11a and b, the increases of surface O_3 level can be seen
 577 in both January and July over the YRD region, with large increase centers occurring in megacities.
 578 In January (Fig. 11a), the maximum O_3 difference appears in Shanghai, with the monthly mean
 579 increment of 2.5ppb (18%). In July (Fig. 11b), the highest O_3 change occurs in Hangzhou, with the
 580 added value of 4 ppb (15%). In the surrounding areas of these high value centers, **increase of O_3**
 581 **associated with the introduction of AH** can be over 0.5 ppb in January and more than 1 ppb in July.
 582 This change pattern and the magnitude are consistent with the findings reported in Beijing (Yu et al.
 583 et al., 2014) and Seoul (Ryu et al., 2013).

584

585 Chemical direct and indirect effects should play a more important role in O_3 changes than
 586 other physical influencing factors. On the one hand, the rising up of air temperature (Fig. 6c and d)
 can directly accelerate O_3 formation by increasing the chemical reaction rates, and thereby

587 straightly increase the O₃ level at surface. On the other hand, O₃ changes are inextricably
 588 influenced by the changes of NO_x (indirect chemical effects). Similar to other primary air pollutant
 589 (such as PM₁₀), NO_x at ground level are reduced in both January and July due mainly to the
 590 increase in PBLH, surface wind speed and upward air movement caused by adding AH (Fig. 11c
 591 and d). It was reported that the O₃ formation over the cities in the YRD region is sensitive to VOC
 592 (Xie et al., 2014), which means that a decrease in surface NO_x might lead to a slight increase of O₃
 593 during the daytime. **At night**, when the process of NO_x titration ($O_3 + NO \rightarrow O_2 + NO_2$)
 594 supersedes the O₃ sensitivity to be the governing factor of O₃ chemistry, less NO_x can only
 595 consume less O₃ as well. Consequently, the decrease in NO_x at the ground can result in the
 596 increase in O₃. This indirect function might be clearly illustrated in vertical distribution of O₃
 597 changes in Sect. 3.4.2.

598



601 **Fig. 11 The spatial distributions of monthly-averaged differences for O₃ and its precursor NO_x between**
 602 **ADDAH and NONAH (ADDAH-NONAH). Differences that are non-significant under the 95% confidence**
 603 **level (student t-test) are masked out.**

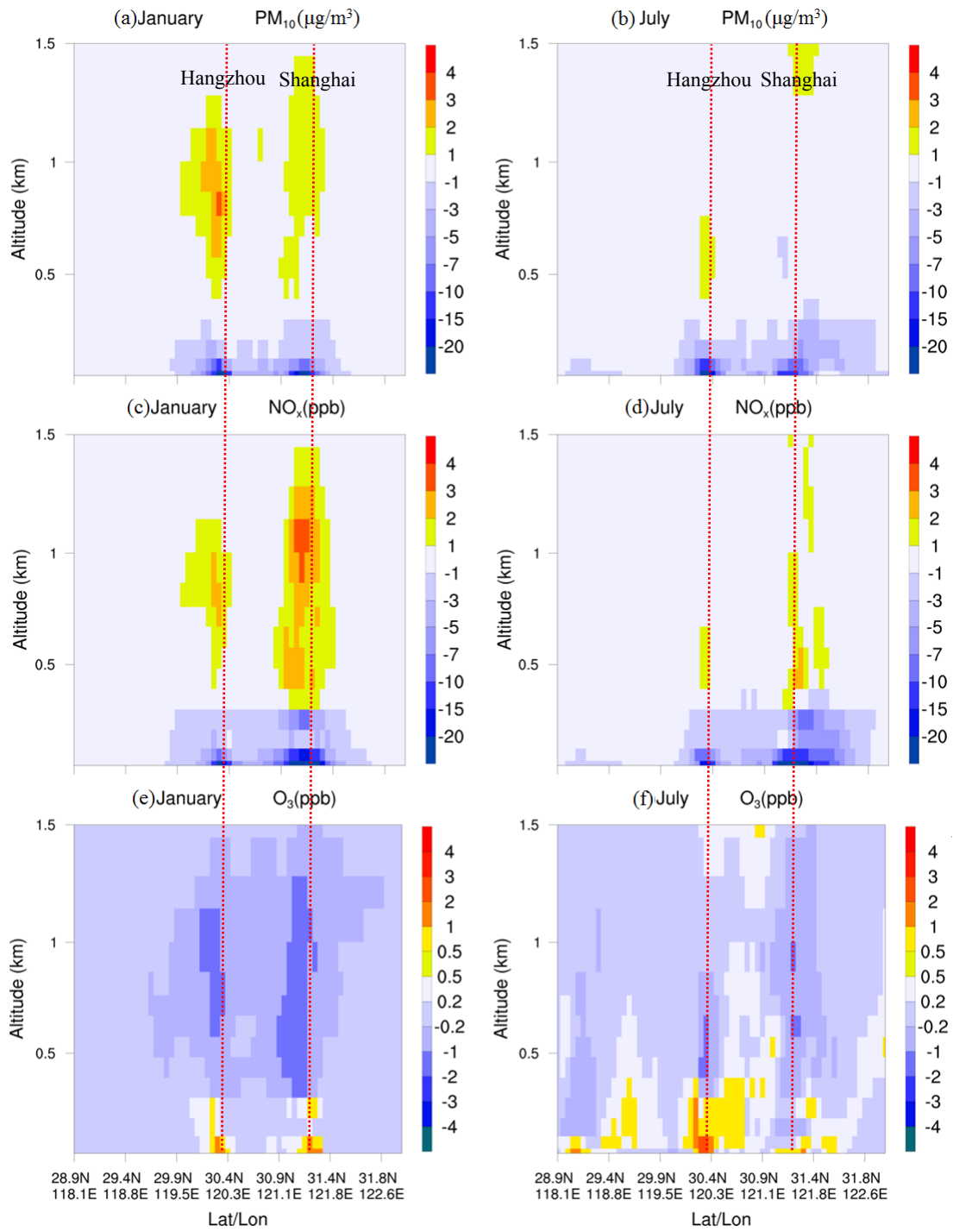
604

605 3.4.2 Vertical changes of PM₁₀ and O₃

606 Fig. 12 shows the vertical plots on the cross-sectional line AB (presented in Fig. 2b) for the
607 changes of chemical species impacted by adding AH (ADDAH-NONAH). Differences that are
608 non-significant at 95% confidence level using t-test have been masked out. For the primary air
609 pollutants such as PM₁₀ and NO_x, the AH fluxes can decrease their concentrations near surface. As
610 shown in Fig. 12a and b, in the atmosphere below 300m above Shanghai and Hangzhou, the
611 concentrations of PM₁₀ decrease 2.3-16.2μg/m³ in January and 2.1-15.8μg/m³ in July, respectively.
612 **Surface** NO_x concentrations near Shanghai and Hangzhou can be reduced over 15 ppb in both
613 month as well (Fig. 12c and d). Meanwhile, it can be also found that there are increases in PM₁₀
614 and NO_x concentrations at the upper levels over the cities. For instance, the added values of PM₁₀
615 and NO_x can be more than 3μg/m³ and 3ppb at about 1km above surface in January, respectively.
616 This vertical changing pattern for primary chemical species is quite similar to that for water vapor
617 (Fig. 9g and h), indicating that this is a reflection of the change in vertical transport patterns in the
618 region due to AH (Yu et al., 2014). It should be noted that the maximum vertical changes of air
619 pollutants in Hangzhou usually occur at about 1km above surface, whereas those in Shanghai
620 generally appear at higher levels (> 1km), implying that more surface air pollutants in Shanghai
621 might be transported into higher levels due to higher AH emissions in this biggest city in the YRD
622 region. Furthermore, Fig. 13 shows the vertical profiles of the changes for PM₁₀, NO_x and O₃
623 caused by adding AH over Shanghai. In winter, the large increases of PM₁₀ and NO_x appear at
624 500m to 1500m above surface. But the maximum increases usually occur at more than 1.5 km
625 above surface in summer. This phenomenon can be attributed to the facts that the atmosphere is
626 more convective in summer than in winter.

627 On the contrary to the primary air pollutants, O₃ changes show increases near surface and
628 decreases at the upper levels over the urban areas. Fig. 12e and f illustrates that the increases of O₃
629 concentrations are limited within 400m above the surface over the cities, with the high values of
630 2.6 ppb in January and 4.2 ppb in July. As mention in Sect. 3.4.1, this may be the result of both the
631 increase in O₃ production caused by higher surface temperature and the decrease in O₃ depletion
632 resulting from less surface NO. With respect to O₃ concentrations from 400m to 1.5km above
633 surface, they generally decrease with the reduction values of more than 1ppb in both January and

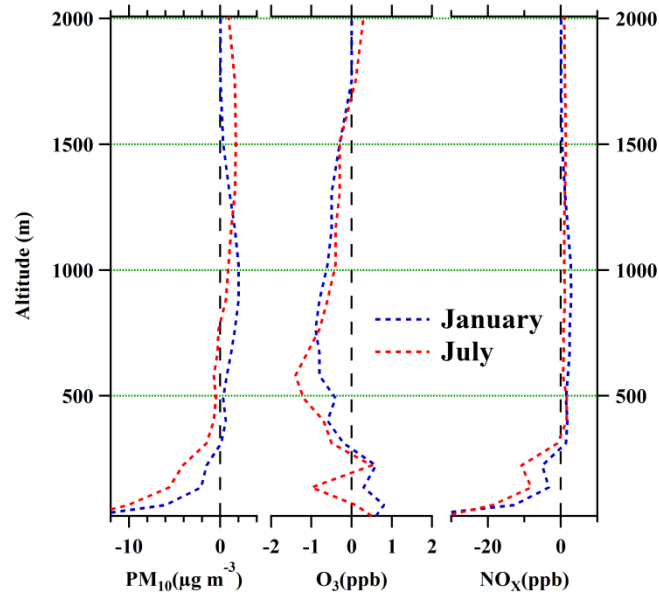
634 July. Comparing Fig. 12e and f with Fig. 12c and d, we believe that the increases of NO_x
635 concentrations at these upper levels can lead to the depletion of O₃, because of the VOC-sensitive
636 O₃ chemistry in the daytime and NO_x titration at night in this region. In some previous studies on
637 the O₃ variations induced by urban land-use, researchers also found that O₃ chemical production is
638 increased at the surface around big cities in summer (Liao et al., 2015; Zhu et al., 2015) and in
639 winter (Liao et al., 2015). However, it was also found that the averaged daytime O₃ in the upper
640 PBL could significantly increase by 20-40ppbv because of strong urban heat island circulation in
641 the summer of Shanghai (Zhu et al., 2015). This result implies that the vertical transport of O₃
642 caused by urban land-use should be stronger than that caused by AH. Thus, more upward O₃ can
643 compensate the depletion of O₃ at upper levels.



644

645 **Fig. 12** The vertical distribution of monthly-averaged differences for PM_{10} , NO_x and O_3 between ADDAH
 646 and NONAH (ADDAH-NONAH) from surface to 1.5km altitude along the line AB (shown in Fig. 2b). (a), (c)
 647 and (e) show changes in January. (b), (d) and (f) illustrate variations in July. Differences that are
 648 non-significant under the 95% confidence level (student t-test) are masked out.

649



650

651 **Fig. 13. The vertical profiles of monthly-averaged differences for PM₁₀, NO_x and O₃ between ADDAH and**
 652 **NONAH (ADDAH-NONAH) over Shanghai.**

653

654 **4. Conclusions**

655 Anthropogenic heat (AH) emissions from human activities caused by urbanization can affect
 656 the city environment. In this paper, we specially address its impacts on meteorological conditions
 657 and air pollution over the cities in the YRD region. Firstly, based on the energy consumption and
 658 the gridded population data, we estimate the spatial distribution of AH fluxes by a top-down
 659 energy inventory method. Secondly, the gridded AH data with the seasonal and the diurnal
 660 variation are added to the sensible heat flux in the modified WRF/Chem. Finally, the WRF/Chem
 661 is applied to investigate the impacts of AH. Two simulation cases are conducted. One incorporates
 662 the single layer urban canopy model (SLUCM) with the gridded AH fluxes, while the other
 663 ignores the contribution of AH.

664 The results show that the AH flux in YRD region has been increased continually since 1990.
 665 During the period between 1990 and 2010, the annual mean values of AH fluxes over Shanghai,
 666 Jiangsu and Zhejiang have been increased from 5.47 to 14.45 W/m², 0.68 to 2.61 W/m², and 0.33
 667 to 1.63 W/m², respectively. High AH fluxes generally occur in and around the cities. The typical
 668 values of AH in 2010 over the urban areas of Shanghai, Jiangsu and Zhejiang can reach 113.5,
 669 50.2 and 39.3 W/m², respectively.

670 The model results of WRF/Chem fit the observational meteorological conditions and air

671 quality very well. Inclusion of the AH can enhance the urban heat island in the cities over the
672 YRD region. 2-m air temperature can be increased by more than 1 °C in January and over 0.5 °C in
673 July. The PBL heights can be increased with the maximum changes of 140m for January and
674 160m for July in Shanghai. The strengthened urban-breeze circulation resulted from adding AH
675 can enhance the 10-m wind speed and the vertical air movement as well. Thus, more moisture is
676 transported from surface to the upper levels, with 0.6g/kg decrease at the ground level and 0.1g/kg
677 increase for the upper PBL in July, which might induce the accumulative precipitation to increase
678 by 15-30% in Shanghai, Nanjing and Hangzhou.

679 Influenced by the modifications of meteorological conditions, the spatial and vertical
680 distribution of air pollutants is **modified**. With respect to the primary air pollutants (PM₁₀ and
681 NO_x), their transport and dispersion in PBL can be facilitated by the increases of PBLH, surface
682 wind speed and upward air movement, which causes the decreases of concentrations near surface
683 and the increases at the upper levels. Usually, PM₁₀ can be reduced by 2-16 µg/m³ within 300m
684 above the surface of the cities, and added over 3µg/m³ in upper PBL. However, surface O₃
685 concentrations increase in the urban areas, with maximum changes of 2.5ppb in January and 4 ppb
686 in July. Besides the rising up of air temperature directly accelerating the surface O₃ formation, the
687 decrease in NO_x at the ground can also result in the increase of surface O₃ due to the
688 VOC-sensitive O₃ chemistry in the daytime and NO_x titration at night in this region. Furthermore,
689 O₃ concentrations at higher levels are reduced by about 1ppb due mainly to the increase of NO,
690 and the impacts of AH are not only limited to the urban centers but also extended regionally.

691 Impact of anthropogenic heat emission on urban climate and air quality is undoubtedly an
692 important and complex scientific issue. Our results show that the meteorology and air pollution
693 predictions in and around large urban areas are highly sensitive to the anthropogenic heat inputs.
694 In a consequent, for further understanding of urban atmospheric environment issues, good
695 information on land use, detailed urban structure of the cities and more studies of the
696 anthropogenic heat release should be better considered.

697

698 **Acknowledgments**

699 This work was supported by the National Natural Science Foundation of China (41475122,
700 91544230), the National Special Fund for Environmental Protection Research in the Public

701 Interest (201409008), Key Laboratory of South China Sea Meteorological Disaster Prevention and
702 Mitigation of Hainan Province (SCSF201401), the National Science Foundation of Jiangsu
703 Province (BE2015151) and EU 7th Framework Marie Curie Actions IRSES project: REQUA
704 (PIRSES-GA-2013-612671). The authors would like to thank the anonymous reviewers for their
705 constructive and precious comments on this manuscript.

706

707 **References**

708 Allen, L., Lindberg, F., and Grimmond, C. S. B.: Global to city scale urban anthropogenic heat flux: model and
709 variability, *International Journal Of Climatology*, 31, 1990-2005, 10.1002/joc.2210, 2011.

710 Block, A., Keuler, K., and Schaller, E.: Impacts of anthropogenic heat on regional climate patterns, *Geophys Res*
711 *Lett*, 31, Artn L12211 10.1029/2004gl019852, 2004.

712 Bohnenstengel, S. I., Hamilton, I., Davies, M., and Belcher, S. E.: Impact of anthropogenic heat emissions on
713 London's temperatures, *Q J Roy Meteor Soc*, 140, 687-698, 10.1002/qj.2144, 2014.

714 Chen, B., Shi, G. Y., Wang, B., Zhao, J. Q., and Tan, S. C.: Estimation of the anthropogenic heat release
715 distribution in China from 1992 to 2009, *Acta Meteorol Sin*, 26, 507-515, 10.1007/s13351-012-0409-y, 2012.

716 Chen, F., and Dudhia, J.: Coupling an advanced land surface-hydrology model with the Penn State-NCAR MM5
717 modeling system. Part I: Model implementation and sensitivity, *Mon Weather Rev*, 129, 569-585, Doi
718 10.1175/1520-0493(2001)129<0569:Caalsh>2.0.Co;2, 2001.

719 Chen, F., Kusaka, H., Bornstein, R., Ching, J., Grimmond, C. S. B., Grossman-Clarke, S., Loridan, T., Manning, K.
720 W., Martilli, A., Miao, S. G., Sailor, D., Salamanca, F. P., Taha, H., Tewari, M., Wang, X. M., Wyszogrodzki, A.
721 A., and Zhang, C. L.: The integrated WRF/urban modelling system: development, evaluation, and applications to
722 urban environmental problems, *International Journal Of Climatology*, 31, 273-288, 10.1002/joc.2158, 2011.

723 Chen, Y., Jiang, W. M., Zhang, N., He, X. F., and Zhou, R. W.: Numerical simulation of the anthropogenic heat
724 effect on urban boundary layer structure, *Theor Appl Climatol*, 97, 123-134, 10.1007/s00704-008-0054-0, 2009.

725 Crutzen, P. J.: New Directions: The growing urban heat and pollution "island" effect - impact on chemistry and
726 climate, *Atmos Environ*, 38, 3539-3540, 10.1016/j.atmosenv.2004.03.032, 2004.

727 Fan, H. L., and Sailor, D. J.: Modeling the impacts of anthropogenic heating on the urban climate of Philadelphia:
728 a comparison of implementations in two PBL schemes, *Atmos Environ*, 39, 73-84,
729 10.1016/j.atmosenv.2004.09.031, 2005.

730 Feng, J. M., Wang, J., and Yan, Z. W.: Impact of Anthropogenic Heat Release on Regional Climate in Three Vast

731 Urban Agglomerations in China, *Adv Atmos Sci*, 31, 363-373, 10.1007/s00376-013-3041-z, 2014.

732 Ferguson, G., and Woodbury, A. D.: Urban heat island in the subsurface, *Geophys Res Lett*, 34, Artn L23713
733 10.1029/2007gl032324, 2007.

734 Flanner, M. G.: Integrating anthropogenic heat flux with global climate models, *Geophys Res Lett*, 36, Artn
735 L02801 10.1029/2008gl036465, 2009.

736 Grimmond, C. S. B.: The Suburban Energy-Balance - Methodological Considerations And Results for a
737 Midlatitude West-Coast City under Winter And Spring Conditions, *International Journal Of Climatology*, 12,
738 481-497, DOI 10.1002/joc.3370120506, 1992.

739 Guenther, A., Karl, T., Harley, P., Wiedinmyer, C., Palmer, P. I., and Geron, C.: Estimates of global terrestrial
740 isoprene emissions using MEGAN (Model of Emissions of Gases and Aerosols from Nature), *Atmos Chem Phys*,
741 6, 3181-3210, 2006.

742 Hamilton, I. G., Davies, M., Steadman, P., Stone, A., Ridley, I., and Evans, S.: The significance of the
743 anthropogenic heat emissions of London's buildings: A comparison against captured shortwave solar radiation,
744 *Build Environ*, 44, 807-817, 10.1016/j.buildenv.2008.05.024, 2009.

745 He, X. F., Jiang, W. M., Chen, Y., and Liu, G.: Numerical simulation of the impacts of anthropogenic heat on the
746 structure of the urban boundary layer, *Chinese J Geophys-Ch*, 50, 74-82, 2007.

747 Iamarino, M., Beevers, S., and Grimmond, C. S. B.: High-resolution (space, time) anthropogenic heat emissions:
748 London 1970-2025, *International Journal Of Climatology*, 32, 1754-1767, 10.1002/joc.2390, 2012.

749 Ichinose, T., Shimodozono, K., and Hanaki, K.: Impact of anthropogenic heat on urban climate in Tokyo, *Atmos*
750 *Environ*, 33, 3897-3909, Doi 10.1016/S1352-2310(99)00132-6, 1999.

751 Janjic, Z. I.: The Step-Mountain Eta Coordinate Model - Further Developments Of the Convection, Viscous
752 Sublayer, And Turbulence Closure Schemes, *Mon Weather Rev*, 122, 927-945, Doi
753 10.1175/1520-0493(1994)122<0927:Tsmecm>2.0.Co;2, 1994.

754 Kain, J. S.: The Kain-Fritsch convective parameterization: An update, *J Appl Meteorol*, 43, 170-181, Doi
755 10.1175/1520-0450(2004)043<0170:Tkcpcu>2.0.Co;2, 2004.

756 Kang, H. Q., Zhu, B., Zhu, T., Sun, J. L., and Ou, J. J.: Impact of Megacity Shanghai on the Urban Heat-Island
757 Effects over the Downstream City Kunshan, *Bound-Lay Meteorol*, 152, 411-426, 10.1007/s10546-014-9927-1,
758 2014.

759 Khan, S. M., and Simpson, R. W.: Effect of a heat island on the meteorology of a complex urban airshed,
760 *Bound-Lay Meteorol*, 100, 487-506, Doi 10.1023/A:1019284332306, 2001.

761 Kikegawa, Y., Genchi, Y., Yoshikado, H., and Kondo, H.: Development of a numerical simulation system toward
762 comprehensive assessments of urban warming countermeasures including their impacts upon the urban
763 buildings' energy-demands, *Appl Energ*, 76, 449-466, 10.1016/S0306-2619(03)00009-6, 2003.

764 Kim, H. J., and Wang, B.: Sensitivity of the WRF Model Simulation of the East Asian Summer Monsoon in 1993
765 to Shortwave Radiation Schemes and Ozone Absorption, *Asia-Pac J Atmos Sci*, 47, 167-180,
766 10.1007/s13143-011-0006-y, 2011.

767 Kusaka, H., and Kimura, F.: Coupling a single-layer urban canopy model with a simple atmospheric model:
768 Impact on urban heat island simulation for an idealized case, *J Meteorol Soc Jpn*, 82, 67-80, Doi
769 10.2151/Jmsj.82.67, 2004.

770 Lee, S. H., Song, C. K., Baik, J. J., and Park, S. U.: Estimation of anthropogenic heat emission in the Gyeong-In
771 region of Korea, *Theor Appl Climatol*, 96, 291-303, 10.1007/s00704-008-0040-6, 2009.

772 Li, L., Chen, C. H., Fu, J. S., Huang, C., Streets, D. G., Huang, H. Y., Zhang, G. F., Wang, Y. J., Jang, C. J., Wang,
773 H. L., Chen, Y. R., and Fu, J. M.: Air quality and emissions in the Yangtze River Delta, China, *Atmos Chem*
774 *Phys*, 11, 1621-1639, 10.5194/acp-11-1621-2011, 2011.

775 Liao, J. B., Wang, T. J., Jiang, Z. Q., Zhuang, B. L., Xie, M., Yin, C. Q., Wang, X. M., Zhu, J. L., Fu, Y., and
776 Zhang, Y.: WRF/Chem modeling of the impacts of urban expansion on regional climate and air pollutants in
777 Yangtze River Delta, China, *Atmos Environ*, 106, 204-214, 10.1016/j.atmosenv.2015.01.059, 2015.

778 Liao, J. B., Wang, T. J., Wang, X. M., Xie, M., Jiang, Z. Q., Huang, X. X., and Zhu, J. L.: Impacts of different
779 urban canopy schemes in WRF/Chem on regional climate and air quality in Yangtze River Delta, China, *Atmos*
780 *Res*, 145, 226-243, 10.1016/j.atmosres.2014.04.005, 2014.

781 Lin, Y. L., Farley, R. D., and Orville, H. D.: Bulk Parameterization Of the Snow Field In a Cloud Model, *J Clim*
782 *Appl Meteorol*, 22, 1065-1092, Doi 10.1175/1520-0450(1983)022<1065:Bpotsf>2.0.Co;2, 1983.

783 Liu, Q., Lam, K. S., Jiang, F., Wang, T. J., Xie, M., Zhuang, B. L., and Jiang, X. Y.: A numerical study of the
784 impact of climate and emission changes on surface ozone over South China in autumn time in 2000-2050, *Atmos*
785 *Environ*, 76, 227-237, 10.1016/j.atmosenv.2013.01.030, 2013.

786 Lu, Y., Wang, Q. G., Zhai, Y. R., Song, Y. Y., Zhang, Y. Y., Sun, P.: Anthropogenic heat emissions in the
787 Yangtze River Delta region, *China Environmental Science*, 34, 295-301, 2014.

788 Menberg, K., Bayer, P., Zosseder, K., Rumohr, S., and Blum, P.: Subsurface urban heat islands in German cities,
789 *Sci Total Environ*, 442, 123-133, 10.1016/j.scitotenv.2012.10.043, 2013.

790 Mlawer, E. J., Taubman, S. J., Brown, P. D., Iacono, M. J., and Clough, S. A.: Radiative transfer for

791 inhomogeneous atmospheres: RRTM, a validated correlated-k model for the longwave, *J Geophys Res-Atmos*,
792 102, 16663-16682, Doi 10.1029/97jd00237, 1997.

793 Offerle, B., Grimmond, C. S. B., and Fortuniak, K.: Heat storage and anthropogenic heat flux in relation to the
794 energy balance of a central European city centre, *International Journal Of Climatology*, 25, 1405-1419,
795 10.1002/joc.1198, 2005.

796 Oke, T. R.: The Urban Energy-Balance, *Prog Phys Geog*, 12, 471-508, Doi 10.1177/030913338801200401, 1988.

797 Pigeon, G., Legain, D., Durand, P., and Masson, V.: Anthropogenic heat release in an old European agglomeration
798 (Toulouse, France), *International Journal Of Climatology*, 27, 1969-1981, 10.1002/joc.1530, 2007.

799 Quah, A. K. L., and Roth, M.: Diurnal and weekly variation of anthropogenic heat emissions in a tropical city,
800 Singapore, *Atmos Environ*, 46, 92-103, 10.1016/j.atmosenv.2011.10.015, 2012.

801 Ryu, Y. H., Baik, J. J., and Lee, S. H.: Effects of anthropogenic heat on ozone air quality in a megacity, *Atmos*
802 *Environ*, 80, 20-30, 10.1016/j.atmosenv.2013.07.053, 2013.

803 Sailor, D. J.: A review of methods for estimating anthropogenic heat and moisture emissions in the urban
804 environment, *International Journal Of Climatology*, 31, 189-199, 10.1002/joc.2106, 2011.

805 Sailor, D. J., and Lu, L.: A top-down methodology for developing diurnal and seasonal anthropogenic heating
806 profiles for urban areas, *Atmos Environ*, 38, 2737-2748, 10.1016/j.atmosenv.2004.01.034, 2004.

807 Streets, D. G., Yarber, K. F., Woo, J. H., and Carmichael, G. R.: Biomass burning in Asia: Annual and seasonal
808 estimates and atmospheric emissions, *Global Biogeochem Cy*, 17, Artn 1099 10.1029/2003gb002040, 2003.

809 Wang, T. J., Jiang, F., Deng, J. J., Shen, Y., Fu, Q. Y., Wang, Q., Fu, Y., Xu, J. H., and Zhang, D. N.: Urban air
810 quality and regional haze weather forecast for Yangtze River Delta region, *Atmos Environ*, 58, 70-83,
811 10.1016/j.atmosenv.2012.01.014, 2012.

812 Wang, X. M., Chen, F., Wu, Z. Y., Zhang, M. G., Tewari, M., Guenther, A., and Wiedinmyer, C.: Impacts of
813 Weather Conditions Modified by Urban Expansion on Surface Ozone: Comparison between the Pearl River
814 Delta and Yangtze River Delta Regions, *Adv Atmos Sci*, 26, 962-972, 10.1007/s00376-009-8001-2, 2009.

815 Wang, X. M., Sun, X. G., Tang, J. P., and Yang, X. Q.: Urbanization-induced regional warming in Yangtze River
816 Delta: potential role of anthropogenic heat release, *Int J Climatol*, 35, 4417-4430, 10.1002/joc.4296, 2015.

817 Wu, K., and Yang, X. Q.: Urbanization and heterogeneous surface warming in eastern China, *Chinese Sci Bull*, 58,
818 1363-1373, 10.1007/s11434-012-5627-8, 2013.

819 Xie, M., Zhu, K. G., Wang, T. J., Yang, H. M., Zhuang, B. L., Li, S., Li, M. G., Zhu, X. S., and Ouyang, Y.:
820 Application of photochemical indicators to evaluate ozone nonlinear chemistry and pollution control

821 countermeasure in China, *Atmos Environ*, 99, 466-473, 10.1016/j.atmosenv.2014.10.013, 2014.

822 Xie, M., Zhu, K. G., Wang, T. J., Feng, W., Zhu, X. S., Chen, F., Ouyang, Y., Liu, Z. J.: Study on the distribution
823 of anthropogenic heat flux over China, *China Environmental Science*, 35, 728-734, 2015.

824 Yang, W. M., Jiang, H., Yu, X. Y., Cui, X. F.: Review of research on anthropogenic heat under climate change,
825 *Progress In Geography* 33, 1029-1038, 2014.

826 Yu, M., Carmichael, G. R., Zhu, T., and Cheng, Y. F.: Sensitivity of predicted pollutant levels to anthropogenic
827 heat emissions in Beijing, *Atmos Environ*, 89, 169-178, 10.1016/j.atmosenv.2014.01.034, 2014.

828 Zaveri, R. A., Easter, R. C., Fast, J. D., and Peters, L. K.: Model for Simulating Aerosol Interactions and
829 Chemistry (MOSAIC), *J Geophys Res-Atmos*, 113, Artn D13204 10.1029/2007jd008782, 2008.

830 Zaveri, R. A., and Peters, L. K.: A new lumped structure photochemical mechanism for large-scale applications, *J*
831 *Geophys Res-Atmos*, 104, 30387-30415, Doi 10.1029/1999jd900876, 1999.

832 Zhang, N., Gao, Z. Q., Wang, X. M., and Chen, Y.: Modeling the impact of urbanization on the local and regional
833 climate in Yangtze River Delta, China, *Theor Appl Climatol*, 102, 331-342, 10.1007/s00704-010-0263-1, 2010.

834 Zhang, Q., Streets, D. G., Carmichael, G. R., He, K. B., Huo, H., Kannari, A., Klimont, Z., Park, I. S., Reddy, S.,
835 Fu, J. S., Chen, D., Duan, L., Lei, Y., Wang, L. T., and Yao, Z. L.: Asian emissions in 2006 for the NASA
836 INTEX-B mission, *Atmos Chem Phys*, 9, 5131-5153, 2009.

837 Zhu, B., Kang, H. Q., Zhu, T., Su, J. F., Hou, X. W., and Gao, J. H.: Impact of Shanghai urban land surface forcing
838 on downstream city ozone chemistry, *J Geophys Res-Atmos*, 120, 4340-4351, 10.1002/2014JD022859, 2015.

839 Zhu, K., Blum, P., Ferguson, G., Balke, K. D., and Bayer, P.: The geothermal potential of urban heat islands,
840 *Environ Res Lett*, 5, Artn 044002 10.1088/1748-9326/5/4/044002, 2010.

841 Zhuang, B. L., Li, S., Wang, T. J., Deng, J. J., Xie, M., Yin, C. Q., and Zhu, J. L.: Direct radiative forcing and
842 climate effects of anthropogenic aerosols with different mixing states over China, *Atmos Environ*, 79, 349-361,
843 10.1016/j.atmosenv.2013.07.004, 2013a.

844 Zhuang, B. L., Liu, Q., Wang, T. J., Yin, C. Q., Li, S., Xie, M., Jiang, F., and Mao, H. T.: Investigation on
845 semi-direct and indirect climate effects of fossil fuel black carbon aerosol over China, *Theor Appl Climatol*, 114,
846 651-672, 10.1007/s00704-013-0862-8, 2013b.